Biotechnology Design

www.cambridge.org/bdn

Full Paper: Biodesign Conference

Cite this article: Quioza C and Zboinska MA (2026). Designing with decay: from environmental transformation to programmed degradation in a yeast-cellulose biohydrogel for circular architectural applications. *Biotechnology Design*. **4**, e10, 1–22. https://doi.org/10.1017/S2977905726100262

Received: 23 February 2026 UTC
Revised: 15 May 2026 UTC
Accepted: 21 May 2026 UTC

Keywords:
biomaterials; microbial hydrogels; biodegradation; material lifecycle; circular architectural design

Corresponding author:
Malgorzata A. Zboinska;
Email: malgorzata.zboinska@chalmers.se

Designing with decay: from environmental transformation to programmed degradation in a yeast-cellulose biohydrogel for circular architectural applications

Constanza Quioza and Malgorzata A. Zboinska

Chalmers University of Technology, Sweden

Abstract

As architectural design paradigms shift from century-lasting, fossil-based construction materials toward regenerative, biogenic solutions with much shorter life cycles, a novel opportunity opens for design with material temporality and transformation. Taking a fully biobased yeast-cellulose-alginate-glycerol composite hydrogel as a case, this study examines how physical and visual properties change under air, soil, and water exposure by measuring mass loss, shrinkage, deformation, embrittlement, and color change in manually and robotically extruded constructs from this material. The results reveal distinct patterns of swelling, contraction, structural distortion, surface brittleness, and chromatic shifts that affect the designs across different exposure conditions. Together, these patterns establish a preliminary knowledge basis for architectural design that could accommodate these transitions, demonstrated in a speculative, conceptual architectural design proposal leveraging transformation and decay as part of the design. By situating material temporality as informative rather than detrimental, the study exemplifies how environmentally responsive biomaterials can support circular architectural biodesign.

Impact statement

This work contributes to biodesign research by providing an empirical, design-situated characterization of how a biobased yeast-cellulose biohydrogel transforms and begins to degrade under environmental exposure to air, soil, and water. Through systematic measurement and observation of mass change, deformation, embrittlement, and chromatic variation, the study generates design-relevant material knowledge that makes time-dependent transformation and decay observable, comparable, and interpretable for design inquiry. The contribution lies in enabling biodesign practice and research through foundational material characterization that supports working with unstable, temporally active biomaterials before full technological material optimization. A speculative architectural pavilion is introduced as a translational artifact, demonstrating how empirically observed material behaviors can be spatially interpreted and discussed within architectural and biodesign contexts. By reframing material instability, temporality, and degradation as legitimate objects of biodesign research and as potential design resources rather than performance failures, the work aligns with biodesign agendas that integrate material experimentation, environmental responsiveness, and circular lifecycle thinking. In this way, the study clarifies the role of systematic material characterization as a critical bridge between emerging biomaterials and future regenerative design applications.

Introduction

Biotechnology-enabled, biobased materials increasingly challenge conventional boundaries between fabrication, performance, and lifecycle transformation in design research. In architecture, this shift intersects with long standing debates on material temporality, where the dominance of permanence has historically limited engagement with materials that transform or decompose over time. However, alternative perspectives also exist that have reframed temporality as an inherent and productive dimension of material practice rather than a limitation to be engineered away (Alonso 2021; Mostafavi and Leatherbarrow 1993). Within this reframing, decay is no longer perceived solely as a failure of durability but as a dynamic parameter that can be purposefully integrated into design processes (Song *et al.* 2024; Stickney 2023). This realignment corresponds with parallel advances in biodesign and materials science, which recognize biodegradation as measurable, ecologically aligned, and potentially programmable behavior. For instance, recent studies in biodegradation of cellulose biocomposites and hydrogel systems (Chen *et al.* 2023; Ilomuanya 2020;

Mukherjee *et al.* 2023; Sannino *et al.* 2009) highlight the relevance of material breakdown across sectors ranging from automotive (Fouad and Farag 2020) and packaging (Anggraini 2025; Han *et al.* 2023) to sensing (Aeby *et al.*, 2023) and agricultural water management (Skrzypczak *et al.* 2020). Within architectural research, biodegradation is often framed through the lens of unpredictability, stemming from the multiplicity of parameters, such as humidity, microbial activity, substrate chemistry, and environmental exposure, that collectively drive degradation kinetics. However, several emerging studies suggested that this unpredictability can be partially structured, enabling designers to work with, rather than against, temporal material behavior (Ercan 2025; Ling 2018; Tai *et al.* 2018).

This reframing of decomposition and material change aligns with established scholarship in material-driven design and materials experience research, where time-dependent material behaviors are understood as design resources rather than deficits. Barati and Karana (2019), building on a broader material-driven design framework, conceptualize material affordances as potentials that emerge through physical, sensory, and temporal change, arguing that ageing, degradation, and transformation are integral to how materials act, are perceived, and acquire meaning over time. In parallel, recent work in human-computer interaction and interaction design has operationalized this position through empirical and practice-based studies of biodegradable, growable, and living materials, explicitly treating material lifecycle dynamics, including swelling, dissolution, softening, biological growth, and disassembly, as active design variables rather than failure modes (Lazaro Vasquez *et al.* 2022; Nicolae *et al.* 2023). Similarly, in biodesign and materials experience research, design-oriented material characterization practices have evolved significantly, with emerging materials explored prior to full technological readiness for market release. In this line of work, empirical investigation serves to understand how evolving and unstable material behaviors, such as growth, degradation, environmental responsiveness, and multisensory qualities, shape design potentials and affordances (Karana *et al.* 2018; Kim *et al.* 2024; Risseeuw *et al.* 2024; Zhou *et al.* 2024). Together, this body of work situates design-oriented explorations of material sensibility, transformation and breakdown as established concerns for biodesign, providing a critical context for the present study, which offers an empirical contribution aimed to support material-centered design explorations of environmentally responsive circular architectural biomaterials.

Despite elevated interest in material-centered design research that engages with notions of transience and breakdown, several knowledge gaps persist. First, there is a deficit of approaches that involve characterization, in settings closely representing unstable real-world conditions, of biodegradation behaviors of emerging biomaterials that are water-based, highly sensitive to ambient environment fluctuations, and thus potentially relevant for temporal or responsive design applications. Second, while previous work has demonstrated how material composition, humidity response, and geometric patterning can induce controlled deformation and decay in bio-composites (Ling 2018; Tai *et al.* 2018), little is known about how such principles translate to specific hydrogel compositions, nor how their decomposition profiles can be systematically documented, compared, and anticipated. Finally, existing architectural applications of bio-based materials predominantly emphasize structural and environmental performance, aesthetics, or fabrication workflows (Chayaamor-Heil *et al.* 2023; Choi and Yi 2024; Malik *et al.* 2020; Napier 2022; Panagiotidou *et al.* 2022), leaving the temporal, degradative phase of material life cycles understudied.

This work addresses these gaps by investigating baseline environmental transformation behaviors of a yeast-cellulose-alginate-glycerol hydrogel, further referred to as a yeast-cellulose biohydrogel (YCBH), designed for additive manufacturing using pressure-actuated 3D extrusion. In our prior work, we established 3D printable YCBH formulations, characterized their mechanical and rheological behavior, shrinkage, and deformation, demonstrated the potential for scaling up to architectural component dimensions, suggested future architectural application domains (Bektas *et al.* 2026a). We have also developed computational design strategies that allow steering the aesthetic material effects toward specific architectural surface qualities via computational design and robotic 3D printing (Bektas *et al.* 2026b). The main benefit of our biohydrogel as a circular architectural material resides in its fully natural composition, featuring only organic components: baker's yeast (Saccharomyces cerevisiae), microfibrillated cellulose (MFC) from forestry waste, sodium alginate from brown algae, and plant-based glycerol. Mixed with water, these components form a hydrogel suspension that is extrudable at room temperature with no heat, and potentially biodegradable. The use of renewable biomass sources, available in large quantities but thus far underutilized, comprising yeast and cellulose, makes the material potentially scalable for applications in buildings, which require large material quantities to satisfy the typical high-volume material demand of construction. The scalability potential of the material arises from the fact that it can be formulated from large quantities of currently underutilized industrial side stream biomasses, namely, large amounts of spent yeast from the brewing industry, and large volumes of cellulose residues from forestry and papermaking. As such, this microbially-enhanced and cellulose fiber-reinforced hydrogel is a novel addition to an established family of biobased hydrogels for applications in design and architecture.

Our preliminary observations suggest that the water-based composition, high humidity sensitivity, and biologically active constituents of the yeast-cellulose biohydrogel make it a compelling model material for exploring temporality in design. This study aims to further confirm and validate these initial observations by systematically characterizing biohydrogel transformations under environmental exposure, to understand and describe how the material transforms and degrades over time, and what architectural design potential such transitions could have. The detailed aims are to: (1) document, compare and establish baseline mass, shape and color changes of yeast-cellulose biohydrogel compared across different architectural exposure scenarios, i.e., indoors, outdoors, and in contact with air, water, and soil; (2) demonstrate how material transformation and decomposition can inform regenerative architectural design thinking, by implementing observations from the experimental study in a speculative design proposal that integrates time-based material change as an operative design parameter.

By framing material transformation and decomposition as a capability rather than a drawback, this study aligns with material-driven and biodesign research agendas that frame time-dependent material behaviors as generative design parameters rather than failure modes. The initial findings are intended to act as a foundation for future research that will leverage biodegradation as a programmable dimension of material behavior, ultimately supporting the development of regenerative, circular architectural systems that work with rather than against natural decay.

https://doi.org/10.1017/S2977905726100262 Published online by Cambridge University Press

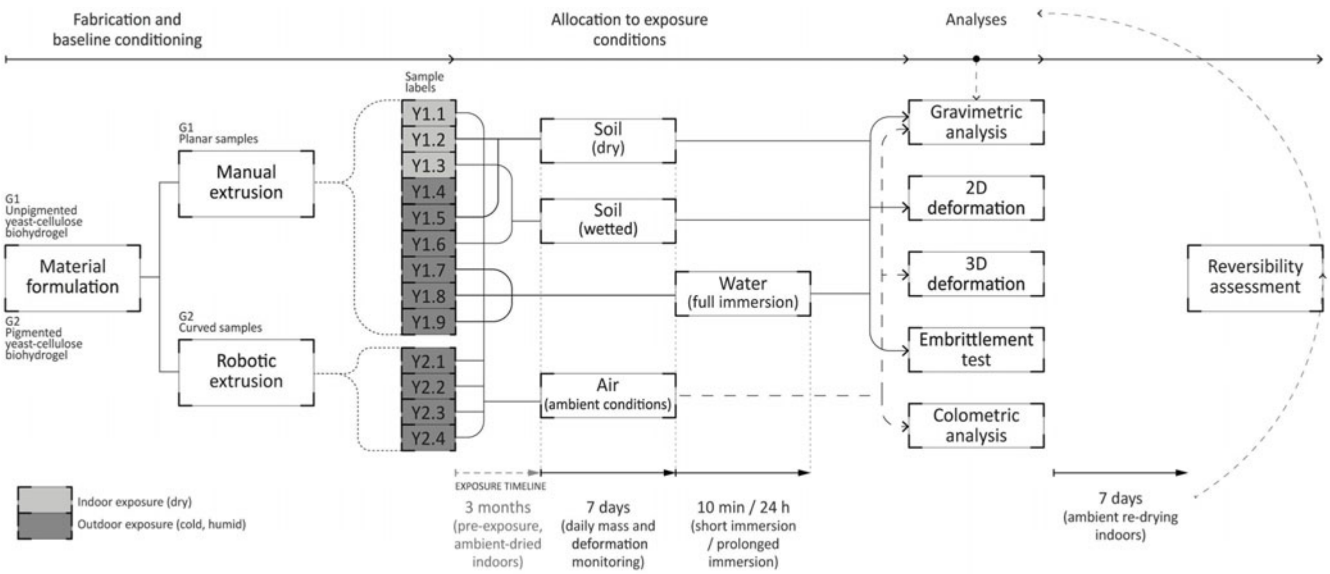

Figure 1. Experimental setup of the study.

Methodology

Material characterization approach

The YCBH material characterization approach in this work follows the biodesign research methodology, where systematic quantitative analysis is combined with qualitative and observational inputs to reveal material properties, behaviors, and transformative tendencies relevant for design. This differs from traditional materials science methods, which prioritize validation of fundamental properties under strictly controlled laboratory conditions and established testing protocols, typically independent of specific design applications and real-life conditions.

Thus, it is not uncommon that some research methods in biodesign encompass new, custom-developed characterization protocols that help capture specific material behaviors as inputs for design-driven inquiry (Crawford 2023). Examples include work that seeks to rigorously characterize the mechanical, physical, and chemical properties of biomaterials while explicitly situating testing within a design-oriented context (Arnardottir *et al.* 2026; Elsacker *et al.* 2019, 2023; Valverde Rojas *et al.* 2026; Zboinska *et al.* 2023). Similarly, within architectural biobased and living materials research, material testing approaches engage with material characterization as a tool facilitating deeper comprehension of behavioral change, environmental coupling, and lifecycle transformation of emerging biomaterials, supporting speculative and translational design work at multiple scales, often with material prototypes and design proposals developed to demonstrate future application potentials and show characterized material properties in action (Dade-Robertson 2020; Stefanova *et al.* 2020).

Following this approach, the experimental procedures in this work were custom-developed to enable baseline yet reproducible material characterization facilitating documentation and understanding of its behaviors. These methods are not intended to deliver a standardized engineering performance specification of the material in question, but to establish fundamental knowledge on how material behavior evolves through interaction with air, soil, water, and climatic exposure over time, with the intent of creating a point of departure for further research and applications.

Experimentation logic

Rather than following strictly controlled laboratory degradation protocols with isolated variables, the study intentionally adopts a comparative exposure logic featuring combinations of different variables and sample typologies, to simulate simplified and reproducible yet close-to-real, and architecturally relevant, material exposure conditions. The overarching goal of this setup was to disclose relations and tendencies between the material response in different baseline sample designs. By structuring the methodology around predefined sample groups, exposure conditions, and exposure durations, the experimental logic aimed to make material transformation pathways directly comparable across environments. This approach supports interpretation of the results as relative, design-informative trends rather than isolated measurements, aligning the methodology with the study's goal of establishing baseline material knowledge for architectural biodesign. Figure 1 shows the global experimental setup for the study following this logic, summarizing sample fabrication, drying and baseline conditioning, allocation to exposure conditions, and measurement timelines.

The environmental exposure logic was meant to represent material exposure scenarios fundamental for architectural applications, encompassing exposure indoors and outdoors, in contact with air, soil, and water. Ambient air exposure was chosen to represent typical atmospheric conditions relevant to interior and exterior architectural applications. Indoor exposure provided a stable baseline exposure scenario with stable humidity and room temperature, while outdoor winter exposure introduced a less stable scenario with fluctuating humidity and temperature close to freezing conditions. Exposure to soil was chosen to represent ground-adjacent or ground-embedded architectural conditions. Dry and wetted soil exposure were devised to compare two typical cases of material interaction, i.e., with dry and wet soil. Finally, direct water exposure through immersion was chosen to represent extreme but architecturally plausible scenarios for material placement in water runoff zones, flooding, and in sacrificial structures intended to biodegrade.

The exposure conditions described above were applied to two YCBH material sample groups (G1, G2) with intentionally

https://doi.org/10.1017/S2977905726100262 Published online by Cambridge University Press

differentiated geometric and fabrication characteristics, specified in the *Sample design* section. The fabrication, conditioning, exposure and analyses of all samples followed a consistent experimental sequence. After material preparation and fabrication, the samples were ambient-dried indoors for three months to ensure a stabilized dry reference state. Thereafter, environmental exposure experiments were conducted under the defined conditions, with regular data collection from measurements and visual documentation. Selected samples were subsequently allowed to re-dry indoors to evaluate reversibility of mass and geometry changes.

Materials and preparation procedures

The YCBH material is a biobased, 3D-printable composite hydrogel developed for lightweight architectural applications, composed of yeast biomass, microfibrillated cellulose (MFC), sodium alginate, glycerol, and water. The material is non-living, and all yeast used in the formulation was oven-deactivated, ensuring biological inactivity, material stability, and compatibility with architectural use while retaining the functional benefit of yeast as rapidly growable microbial biomass.

Yeast *(Saccharomyces cerevisiae)* is included in the formulation as a primary biogenic component due to its exceptional abundance, scalability, and low environmental footprint (Bektas *et al.* 2026a). In the deactivated state, yeast contributes structurally rather than biologically. Depending on cell state, yeast acts either as a filler (intact cells) or as a binder (homogenized cells releasing intracellular proteins, carbohydrates, and lipids), enhancing cohesion and toughness of the hydrogel matrix. Unlike filamentous fungal mycelium, yeast is unicellular, enabling homogeneous material formation, reduced contamination risk, and compatibility with direct extrusion-based fabrication, which are critical for architectural-scale applications. It also grows and forms biomass much faster than mycelium, at an exponential rate, with a few milligrams of starter culture able to multiply into several tons of biomass within a week in industrial bioreactors.

Microfibrillated cellulose (MFC) serves as the primary structural and rheological scaffold, providing shear-thinning behavior, shape fidelity after extrusion, and mechanical reinforcement upon drying. MFC is renewable, widely available from forestry side streams, and has been established as a promising biobased material for sustainable architectural applications (Rudin *et al.* 2022; Zboinska 2025; Zboinska *et al.* 2023). Sodium alginate is introduced as a gel-forming and viscosity-modulating agent, supporting extrusion stability and reducing deformation during drying. Glycerol functions as a plasticizer, improving flexibility, crack resistance, and moisture retention, which are key properties for lightweight, thin-sheet architectural materials for use in interior claddings, room divider screens, and wall finishes. Water acts as the dispersion and processing medium, enabling ingredient suspension to form the hydrogel matrix and facilitating extrusion-based fabrication at ambient-temperature, without thermal curing.

Together, this ingredient system is conceived to align sustainability, design freedom, and digital fabrication requirements in architecture by relying on renewable and biodegradable constituents, enabling robotic 3D printing at room conditions, and yielding tunable properties, including translucency, texture, and deformation tolerance, relevant for non-loadbearing architectural components.

Based on this formulation design logic, the YCBH formulation in this study corresponds to YO20-MFC10-ALG-GLY formulation reported in Bektas *et al.* (2026a), comprising 3% (w/v) oven-deactivated yeast, 13% aqueous MFC solution (from a 10% microfibril suspension), 1% sodium alginate, 5% glycerol, and 78% water. In sample group G2, edible powdered food pigments (Squires Kitchen, United Kingdom) were added to the hydrogel in quantities given in Table S1 in the Supplementary file, to enable controlled coloration without altering material behavior. Pigments were weighed using a calibrated digital scale (Diyife BHMK4, accuracy ± 0.01 g), added to the hydrogel, and manually mixed with a silicone spatula until visually homogeneous.

Sample design

Two groups of YCBH samples, G1 and G2, were designed to address different research objectives (Figure 2). Sample shapes and geometries were deliberately varied between these groups, not for direct comparison, but to assess how mass change and shrinkage kinetics display across different boundary conditions and morphologies. The first group (G1) comprised nine manually extruded, flat, square and triangular samples (Y1.1–Y1.9) with outer boundary dimensions ranging from 30 mm × 30 mm to 30 mm × 70 mm. The aim of these samples was to examine two-dimensional (planar) deformation, mass changes and material embrittlement under environmental exposure to outdoor air, soil and full immersion in water.

The second group (G2) included four samples (Y2.1–Y2.4), designed with more complex, curved geometry, pigmented, and with outer boundary dimensions 100 mm × 150 mm. These samples were produced through pressure-based robotic material extrusion onto curved molds. The objective of this group was to examine three-dimensional geometric deformation, mass changes, and chromatic transformation in an ambient outdoor environment to get a preliminary understanding of transformations in more complex construct designs, representing an expanded repertoire of architectural shapes that could be relevant for shaping self-supporting building skins and geometrically complex spatial systems. The curved geometry of these samples was also developed to evaluate whether designs featuring single and double curvatures differ in spatial deformation and shape retention effects.

Robotic material extrusion paths for fabrication of samples in G2 were designed in the digital modeling software Rhinoceros 3D version 7 as parametric curves, generated using add-ins Grasshopper and Karamba3D. Two samples featured rhomboid lattice deposition patterns overlaid with parallel linear striations, projected onto a single-curved geometry. Two other ones featured a design based on principal force lines derived from and following a double-curved geometry.

Sample fabrication

The G1 samples were manually extruded using a syringe with a tapered 2.00 mm dispensing tip onto a flat silicone sheet and left to dry. The G2 samples were additively manufactured using robotic extrusion onto 3D printed curved molds, one representing a single and one a double curvature (Figure 3). The molds were 3D modeled in Rhinoceros 3D and 3D printed using PLA filament with the Prusa Slicer MK4 printer.

For the hydrogel 3D printing procedure, the parametric material extrusion paths designed at the outset using Grasshopper and Karamba3D were translated into points and planes and used as input for generating the robotic extrusion sequence commands using the parametric robot control add-in KUKA|prc version 09.10.2022. Custom parametric sequences in Grasshopper and

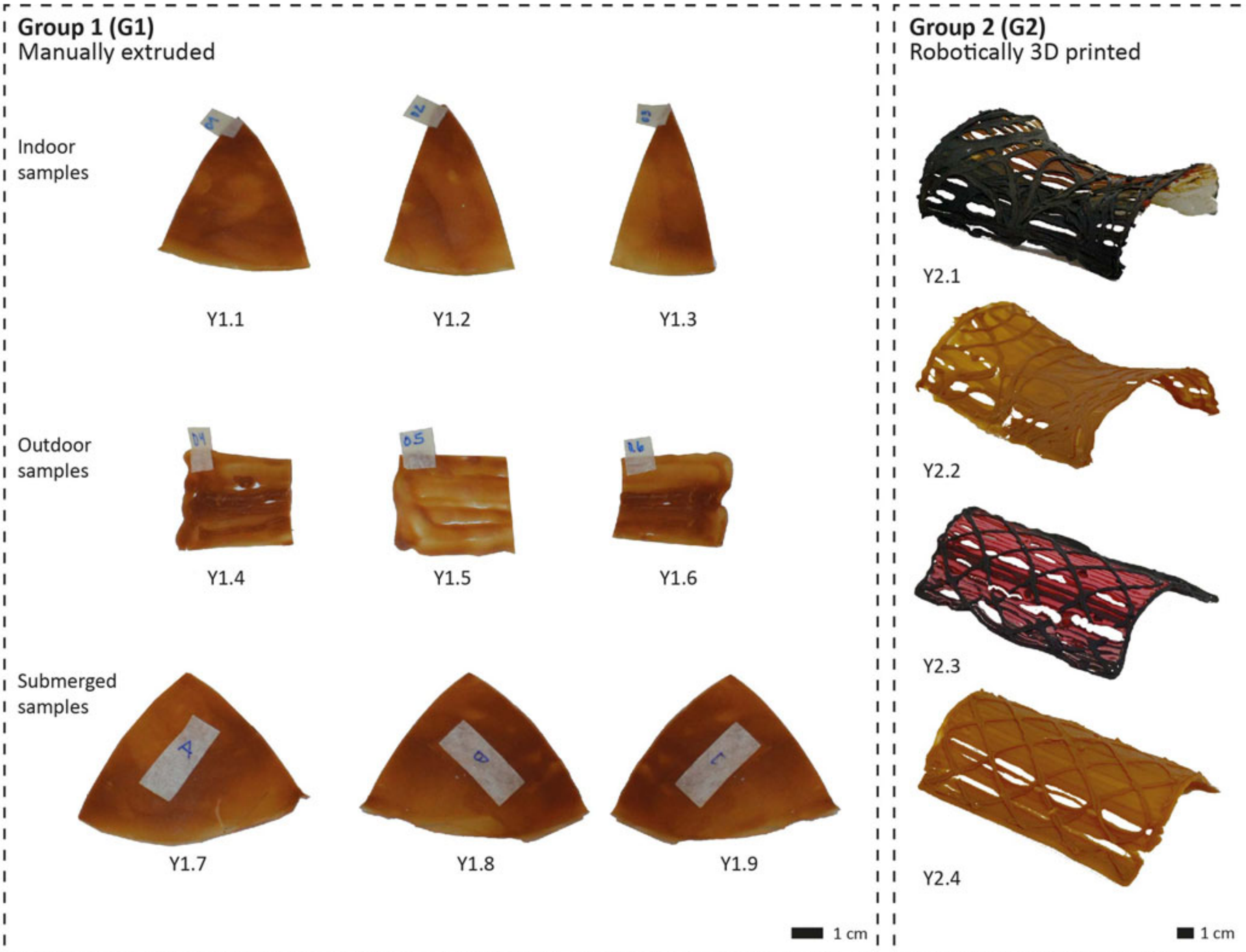

Figure 2. YCBH material sample groups analyzed in the experiments.

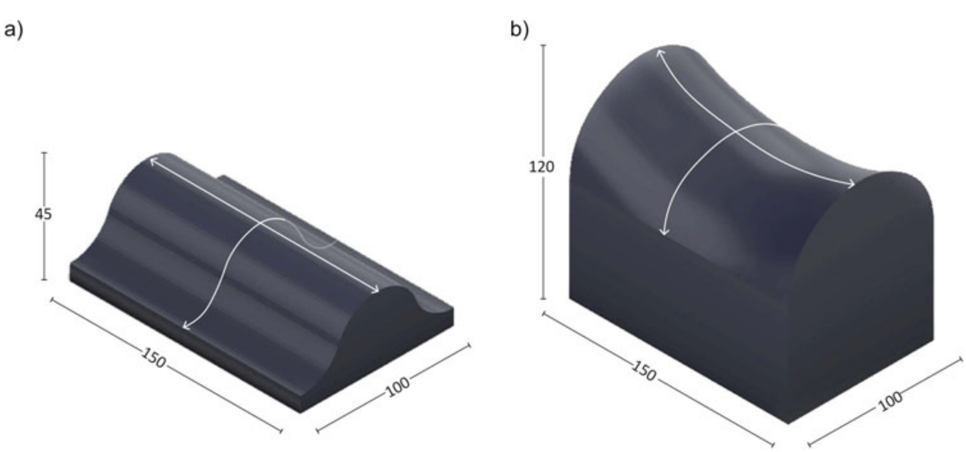

Figure 3. Molds for non-planar robotic extrusion of (a) single-curved, and (b) double-curved YCBH samples.

KUKA|prc were developed to handle plane definition, rotation logic, and collision avoidance through parametrically defined collision zone constraints. The robot used for G2 sample fabrication was the KUKA Agilus KR10 R1100 sixx, equipped with a custom pressure-based extrusion system shown in Figure 4 and described in detail in Zboinska *et al.* (2023). The extrusion pressure ranges were 0.2–1.0 bar, and the dispensing tip diameter was 2.50 mm.

https://doi.org/10.1017/S2977905726100262 Published online by Cambridge University Press

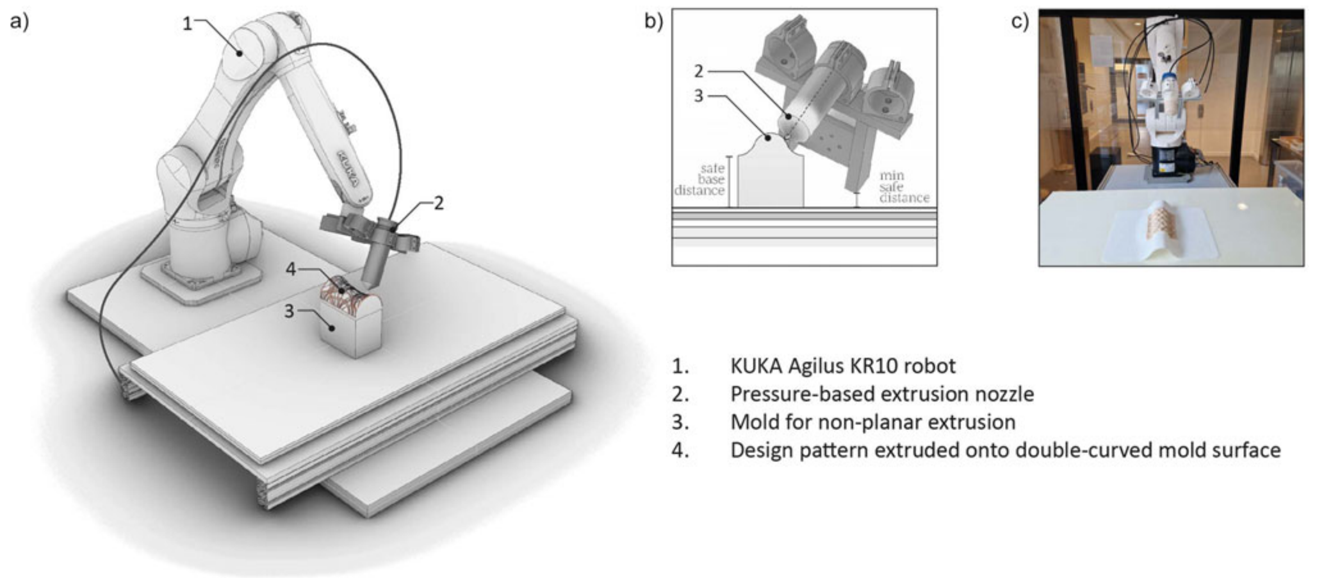

Figure 4. YCBH material extrusion setups onto curved molds: (a) robot cell elements, (b) collision avoidance constraints applied in robot end-effector tilt, (c) physical robot cell for process execution.

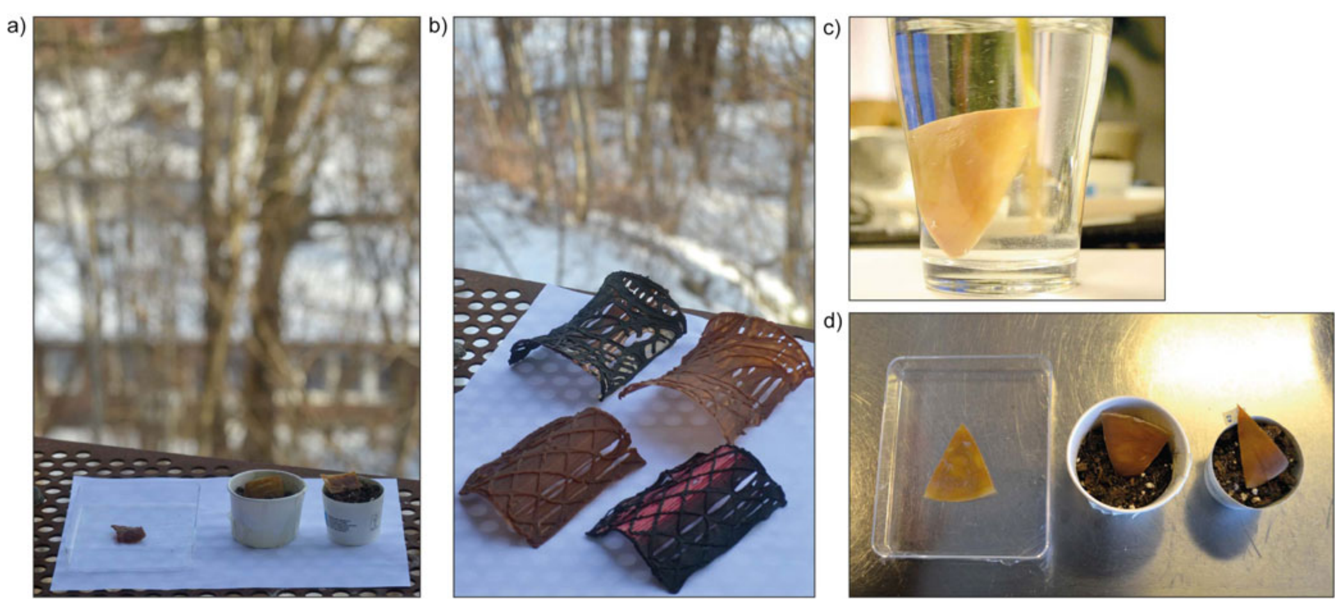

Figure 5. YCBH samples in key exposure conditions: (a) outdoors on plastic tray, dry soil, and wet soil; (b) outdoors on plastic underlay; (c) fully immersed in water; and d) indoors on plastic underlay, dry soil, and wet soil.

After extrusion, all material samples were air-dried in ambient indoor conditions (temperature 21.8°C ± 0.5°C, relative humidity 30.5% ± 4.4%). All samples were stored indoors for three months prior to environmental exposure experiments.

Environmental exposure and gravimetric analysis

Gravimetric analysis of YCBH sample mass changes was conducted across divergent environmental regimes to quantify biomaterial hydration kinetics under contrasting boundary conditions. The indoor exposure experiments simulated a temperate climate (Köppen BWk; 22°C ± 0.5°C, 30.5% ± 4.4% RH), while outdoor measurements captured transient cold humid continental climate (Köppen Dfb-like; −5°C ± 0.5°C, 70% ± 5% RH) during winter.

The nine material samples from G1 were used to compare sample transformations in these ambient outdoor and indoor environments (Figure 5). Further, they were also examined in contact with soil and water to understand interactions with these media. Three samples (Y1.4, Y1.5, Y1.6) were left outdoors with the protection of a metal strainer to prevent animal interference. Sample Y1.4 was placed directly on a plastic tray, Y1.5 on top of soil, and Y1.6 on top of soil wetted daily with water until visible soil saturation was achieved. Samples Y1.1, Y1.2, and Y1.3 were kept indoors without protection. Sample Y1.1 was left on top of a plastic tray; sample Y1.2 was placed directly on top of soil and Y1.3 on soil

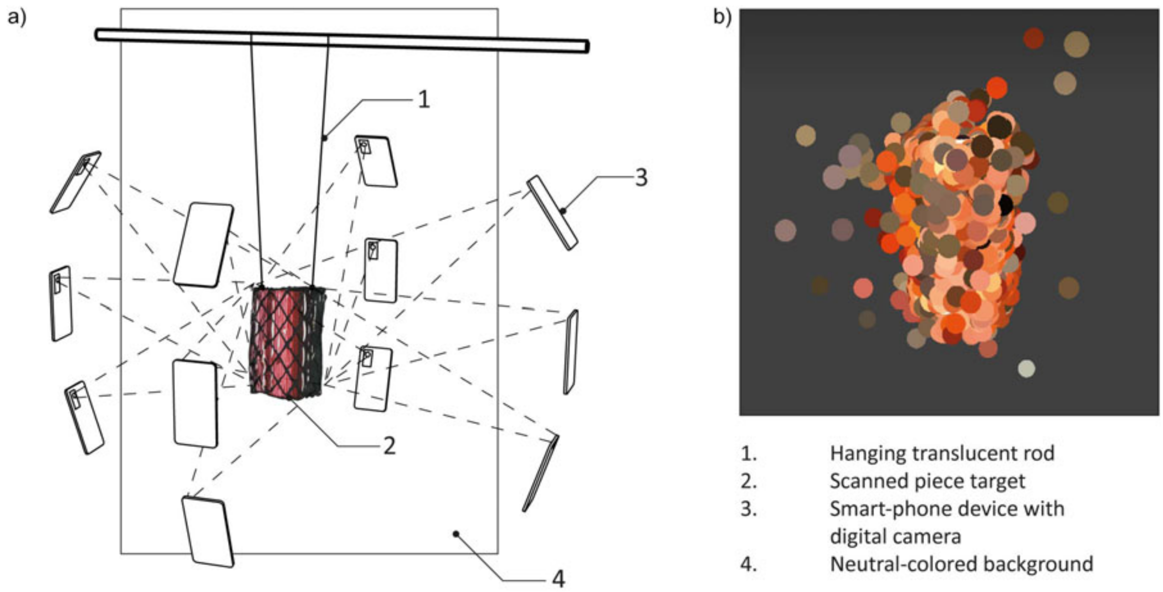

Figure 6. (a) Photography setup for photogrammetry-based scanning of curved YCBH samples, (b) raw scan data in the Scaniverse app.

with daily water addition. The soil used was the KRAV-certified sowing soil. Indoor and outdoor samples were monitored for seven days and weighed once per day.

The last three samples (Y1.7, Y1.8, Y1.9) were immersed in municipal tap water from Gothenburg, Sweden (Lackarebäck and Alelyckan treatment plants), characterized by a low mineral content with a median total hardness of 20–22 mg/L and a slightly alkaline median pH of 7.9–8.0. Sample Y1.7 was submerged in 250 ml of water in a glass vessel and subjected to manual stirring with a rod for 10 minutes, directly followed by mass measurements. Sample Y1.8 was submerged in 250 ml of water without stirring for 10 minutes and then weighed. Sample Y1.9 was immersed in the same way as sample Y1.8 but remained submerged for 24 hours before weighing.

The four robotically 3D printed samples from G2 (Y2.1–Y2.4) were exposed to the same outdoor weather conditions as the G1 outdoor samples, placed on a white paper sheet (density 80 g/m^2) and covered with a metal strainer to prevent animal interference. All samples were weighed again after seven days of ambient drying indoors to evaluate mass changes.

Mass measurements were performed using a digital scale Diyife BHMK4 with auto-calibration, capacity of 500 g, and accuracy of 0.01 g. Ambient temperature and relative humidity during the experiments were monitored using a digital thermometer-hygrometer (Hygrometer 026013), with an operating temperature range of 0–50°C and relative humidity range 0–100% RH.

Gravimetric analysis was conducted to quantify mass change over time, where the percentage change in mass (Δm) at each measurement point was calculated using Equation (1)

$$\Delta m = \frac{m_t - m_0}{m_0} \times 100 \quad (1)$$

where m_0 is the initial mass and m_t is the mass at time t. Positive values indicate mass gain due to moisture absorption, while negative values indicate mass loss due to drying.

Deformation analyses

Thickness measurements were performed using an analog caliper. Two-dimensional deformation was quantified through comparative analyses of enclosed projected areas. Each G1 sample was projected onto a white paper background by manually tracing its perimeter with a 0.05 mm pencil. The traced contours were subsequently digitized and analyzed in AutoCAD 2D to compute the enclosed area. Deformation was expressed as percentage change with respect to the initial projected area.

Three-dimensional deformation in G2 samples was analyzed by comparing the distances between digital scans of physical samples acquired using photogrammetry. Each sample was placed against a neutral white background in uniform illumination to minimize shadows. For greater scanning accuracy, samples were suspended using transparent fishing lines and photographed from multiple distances and angles (Figure 6). Images were captured with an iPhone XR (12-megapixel wide-angle camera with optical image stabilization) and converted to digital 3D mesh models using the Scaniverse app. Each 3D printed sample was scanned twice: first after three months of drying following 3D printing (1), and on the seventh day of outdoor exposure (2).

After environmental exposure, the samples were digitally compared with the initial pre-exposed state in the Rhinoceros 3D environment (Figure 7). The originally scanned digital samples (1) and the samples scanned after outdoor exposure (2) were aligned using a closest-point registration to ensure spatial accuracy for deviation analysis. Using the parametric design add-in Grasshopper in Rhinoceros 3D, the point mesh of scanned samples (1) was projected onto the scanned surface (2), as illustrated in Figure 7.

Average distances between corresponding points were calculated and normalized by dividing by the average distance between the original sample (1) points and their centroid. Average model deformation (D) was calculated using Equation (2)

$$D = \frac{dist\ (P_{scan\ 2},\ \ P_{scan\ 1})}{dist\ (P_{scan\ 1},\ \ C_{scan\ 1})} \times 100 \quad (2)$$

https://doi.org/10.1017/S2977905726100262 Published online by Cambridge University Press

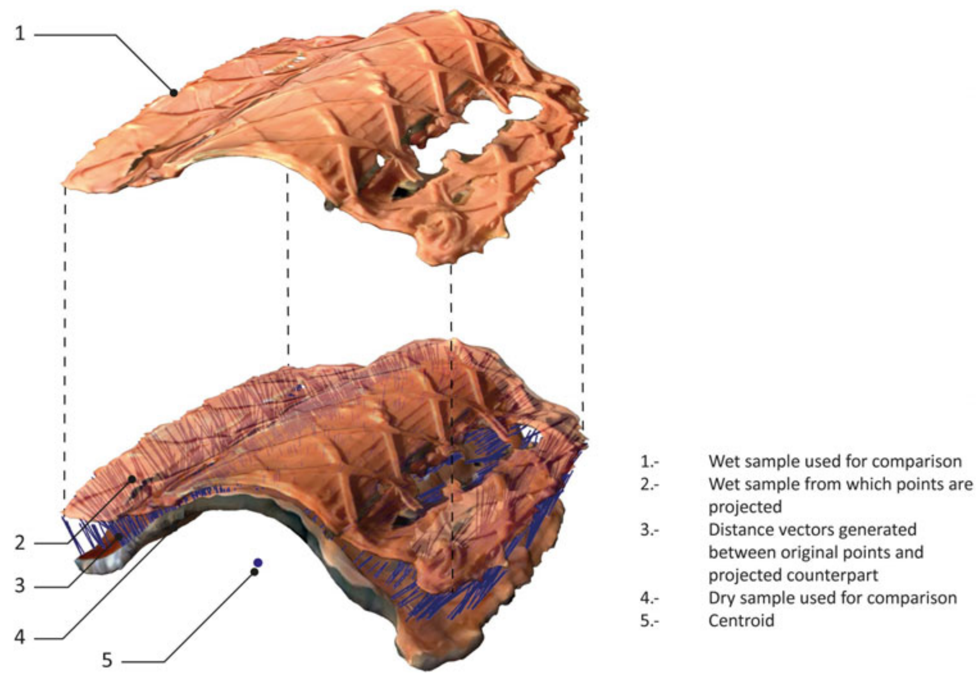

Figure 7. Digital 3D shape deviation analysis based on distance measurements between YCBH samples captured before and after environmental exposure.

where dist ($P_{\text{scan 2}}$, $P_{\text{scan 1}}$) denotes the distance between corresponding points of the model scanned after outdoor exposure (2) and the initial scanned model (1), and dist ($P_{\text{scan 1}}$, $C_{\text{scan 1}}$) denotes the distance between the points of the initial scanned model and its centroid. The resulting normalized ratio, multiplied by 100, defines the deformation percentage.

Embrittlement test

A flexural embrittlement assessment was conducted to evaluate changes in curvature tolerance following environmental exposure. Samples (Y1.1–Y1.9) were subjected to an identical imposed curvature using a fixed-radius cylindrical support. Each sample was bent over an aluminum tube with a radius of 3 mm and maintained in position for 10 seconds. The imposed surface strain during bending was approximated according to classical bending theory and calculated using Equation (3)

$$\varepsilon = \frac{t}{2R} \tag{3}$$

where t corresponds to sample thickness and R to the bending radius. Failure was defined as the appearance of no visible cracking, visible cracking, and fracture.

Colorimetric analysis

To establish color variations, digital photographs of the samples were taken prior to and after environmental exposure. The photographs were captured using a Nikon D3100 DSLR camera with an AF-S DX Nikkor 18–55 mm f/3.5–5.6 G lens. Manual exposure settings were standardized, with aperture *f*/5 and shutter speed 1/80 s. All photographs were taken at a native resolution of 4608 × 3072 pixels. To ensure image acquisition consistency, the camera was mounted on a tripod at a fixed distance of 50 cm from the surface on which the sample was placed, maintaining a near-nadir orientation (angled between 85° and 90°) relative to the sample surface. Further, constant illumination was achieved by using a warm white (3000 K) LED light source with illuminance of 1175 lux, monitored using a NEO NAS-TH02BH sensor. To facilitate white point detection, each sample was placed on a white paper background (density 80 g/m^2, CIE whiteness 160).

Thereafter, to ensure chromatic consistency, digital photographs of the samples were normalized using a white point reference calibration in Adobe Photoshop CC 2017.1.1. Color sampling point locations for each material sample were chosen to represent homogeneous color zones, avoiding edges, shadows, and surface irregularities to ensure comparability between conditions. The points were positioned using a digital ruler tool in Photoshop and further guided by the visible characteristics of the robotically extruded material lines in the samples, whose surface landmarks allowed for consistent point placement for pre-and post-exposure states. Color values for each sampling point were extracted using a 5 × 5 average sample size in Photoshop. The CIELAB color space parameters, i.e., lightness (L), chromaticity in channel (a) representing the red-green color axis, and chromaticity in channel (b) representing the yellow-blue axis, were evaluated using the Eyedropper tool in Photoshop to quantify color transformations. Thereafter, for each sample, LAB values were sampled, and a comparative analysis of color values was conducted. The resulting dataset documents color transformations before and after environmental exposure. The cumulative chromatic shift of the samples, expressed as color difference (ΔE) was calculated using Equation (4)

$$\Delta E^* = \sqrt{(\Delta L^*)^2 + (\Delta a^*)^2 + (\Delta b^*)^2} \tag{4}$$

where L denotes lightness value, a denotes chromaticity channel a value, b denotes chromaticity channel b value, and

$$\Delta L^* = L^*_{wet} - L^*_{dry} \tag{5}$$

$$\Delta a^* = a^*_{wet} - a^*_{dry} \tag{6}$$

https://doi.org/10.1017/S2977905726100262 Published online by Cambridge University Press

$$\Delta b^* = b^*_{wet} - b^*_{dry} \quad (7)$$

This metric integrates changes in lightness and chromaticity, providing a single numerical value that represents the perceptibility of color transformation in the material. The calculated values were interpreted based on the following standard perceptibility thresholds to quantify the material's visual transformation (Mokrzycki and Tatol 2011):

- $\Delta E < 1.0$: Imperceptible; no discernible color change to the human eye.
- $1.0 < \Delta E < 3.5$: Perceptible difference, ranging from visible only to experienced observers to clearly noticeable.
- $\Delta E > 5.0$: Observer perceives two distinct colors.

Results

Because each exposure condition discussed in this section was represented by a single sample, the results below focus on individual sample-specific effects and probable tendencies of the YCBH material rather than its final, statistically validated, and generalizable performance metrics. Further, because temperature and relative humidity varied across measurement days, the results should be interpreted in relation to these environmental fluctuations, which cannot be isolated from each other in the present experimental setup. While several material responses reported in the sections below, including moisture-driven swelling, mass fluctuation, and color change, might be at least partially reversible at the early stages of environmental material exposure, these responses should not be interpreted as final material states. Rather, we speculate that they constitute transitional behaviors that condition, signal, and spatially localize the onset of irreversible decay and degradation of the material, which are to be anticipated under prolonged or intensified environmental exposure.

Mass change behaviors

For manually extruded YCBH samples exposed to indoor conditions (Y1.1, Y1.2, Y1.3), each sample presented distinct behaviors (Figure 8a, Table S2 in the Supplementary file). Sample Y1.1 showed no variation in mass throughout the testing period, despite fluctuations in indoor temperature and humidity. Across the indoor testing period, temperature remained within approximately 21–23.7°C, while relative humidity fluctuated between approximately 19%–35%, indicating moderate environmental variation despite overall stable conditions. Sample Y1.2 exhibited a relative mass increase of 4% on day 1 of exposure, coinciding with a change in measured temperature and humidity, thereafter presenting a drop in mass toward the initial value, with only minor fluctuations (±1%) on the following days. Sample Y1.3, which was partially in contact with moist soil, showed the largest mass changes, with a peak relative mass increase of 18% on day 1, followed by a gradual decrease below its initial mass by the end of the seventh day. On the fourteenth day, samples Y1.1 and Y1.3 exhibited a decrease in relation to initial mass, while sample Y1.2 has shown a slight (2%) relative mass increase. Although a direct causal relationship between mass change, temperature, and humidity cannot be established given the limited sample size and coupled variation of environmental parameters, the results suggest that YCBH exposure indoors to moderate ambient changes might not be sufficient to drive substantial changes to its mass, potentially indicating stable material behavior in these conditions. On the other hand, exposure to wetted soil in these ambient conditions might be a more pronounced cause of larger mass fluctuations.

All three of the manually extruded samples exposed outdoors (Y1.4, Y1.5, Y1.6) exhibited gradual mass gain when exposed to air humidity levels above 50% during the testing period, with a mass gain peak at 84% humidity on the last day of exposure (Figure 8b, Table S3 in the Supplementary file). Although mass increase broadly coincided with rising humidity levels during the observation period, the correspondence is not strictly monotonic across all samples and days. The mass gain occurred for all samples even though they were placed on different substrates, indicating a trend of mass rise potentially correlated with increasing exposure time. Sample Y1.4, which was placed on a plastic substrate, showed a 43% increase in mass. For Y1.5, placed on dry soil, the increase was lower (+35%), likely due to moisture sharing with the substrate. Sample Y1.6, placed on soil wetted once per day exhibited the highest mass gain (+53%), which indicates a moisture absorption tendency of the material. After being left to dry indoors for seven days, all samples exhibited a partial recovery of mass. These observations, although not statistically validated, could indicate a moisture buffering capacity and partial reversibility of moisture uptake of the YCBH material. It should also be noted that outdoor exposure conditions combined elevated humidity with sub-zero temperatures, and the experimental setup did not allow clear isolation of the respective contributions of temperature and humidity to the observed mass changes. Accordingly, the increased mass observed under outdoor exposure should be understood as a response to combined climatic conditions rather than to humidity alone, as increases in mass coincide with both high relative humidity levels (up to 84%) and sub-zero temperatures, whose individual effects cannot be disentangled in this setup.

Regarding soil interaction behaviors, samples Y1.3 (indoor exposure) and Y1.6 (outdoor exposure), both placed on soil that was wetted daily with water, exhibited visible swelling at the base in contact with the substrate (Figure 9). This suggests capillary moisture transfer between the soil and the material, pointing at the possibility of a dynamic two-way response of the material to moisture fluctuations in contact with wet solid matter, reflected in moisture uptake and moisture release (Zowada and Foudazi 2023).

For the robotically 3D printed samples from G2, exposed to outdoor conditions (Y2.1, Y2.2, Y2.3, and Y2.4; Figure 8c, Table S4 in the Supplementary file), similar to the manually extruded samples from G1, a gradual mass gain trend was observed. During the monitoring period, temperature remained relatively stable (−7°C to −2°C), while humidity fluctuated between approximately 58%–84%, indicating partial decoupling of these parameters compared to G1 outdoor dataset. The curves representing mass increase for G2 samples were steeper than the curves for G1 samples, indicating a potential correlation with sample thickness and rate of moisture uptake, which in the G2 samples could have been larger due to the presence of multiple extrusion layers. The observed mass gain behavior of more rapid moisture intake for robotically extruded compared with the manually extruded samples might also relate to fabrication method-dependent differences in porosity and material homogeneity. The manually extruded samples were less uniform than robotically fabricated ones, which might have affected their mass gain behaviors. However, this interpretation remains tentative given that each condition was represented by a single specimen, and the temperature and humidity varied significantly between the testing scenarios. Nevertheless, the robotically printed samples appeared more compact and homogeneous, which most likely affected their moisture absorption behavior (Pettinelli *et al.* 2024;

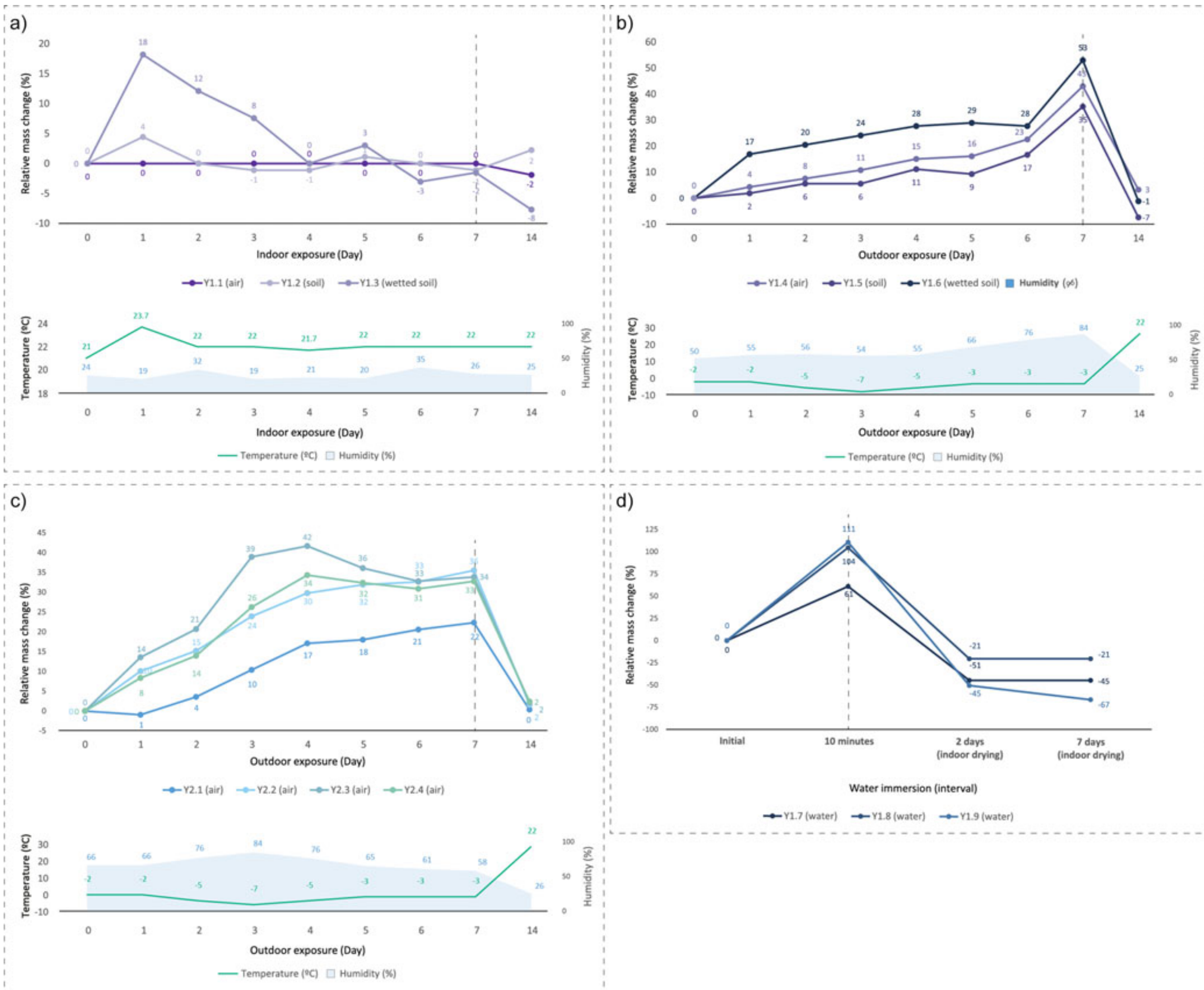

Figure 8. Mass changes and environmental exposure conditions over time for G1 and G2 samples placed: (a) indoors, exposed to air, dry soil and wetted soil; (b) outdoors, exposed to air, dry soil and wetted soil; (c) outdoors, exposed to air; (d) immersed in water. Dashed vertical line in each graph denotes transition to indoor/drying phase.

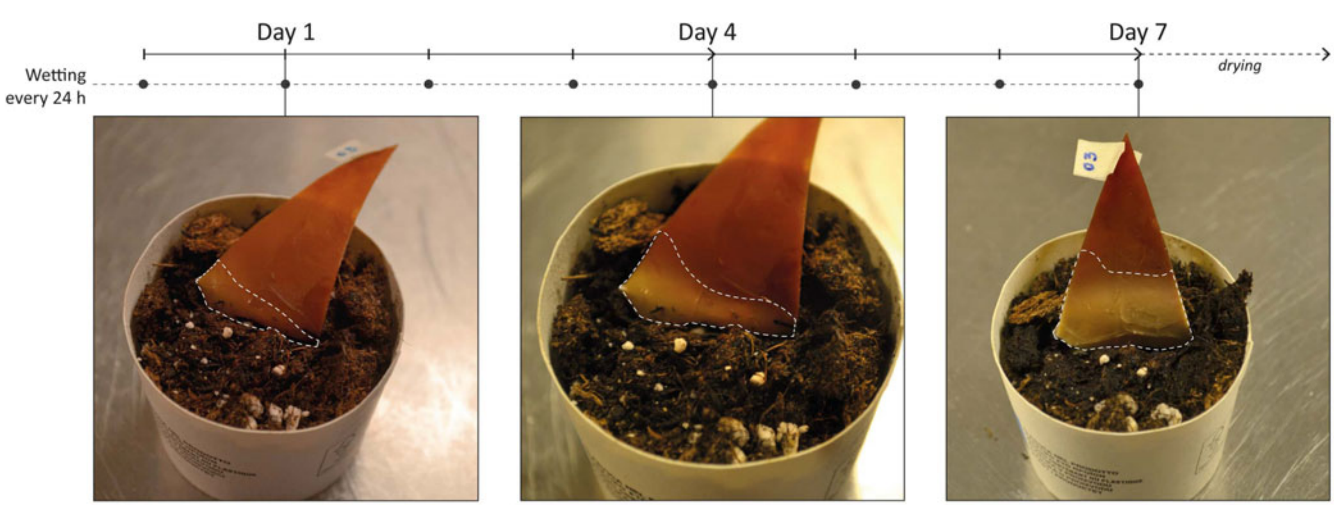

Figure 9. Moisture uptake phenomena occurring in YCBH material under seven days of sample exposure to contact with wetted soil. Wetting was done every 24 hours. Dashed outlines show increase and lighter sample color show zones of moisture uptake in the material.

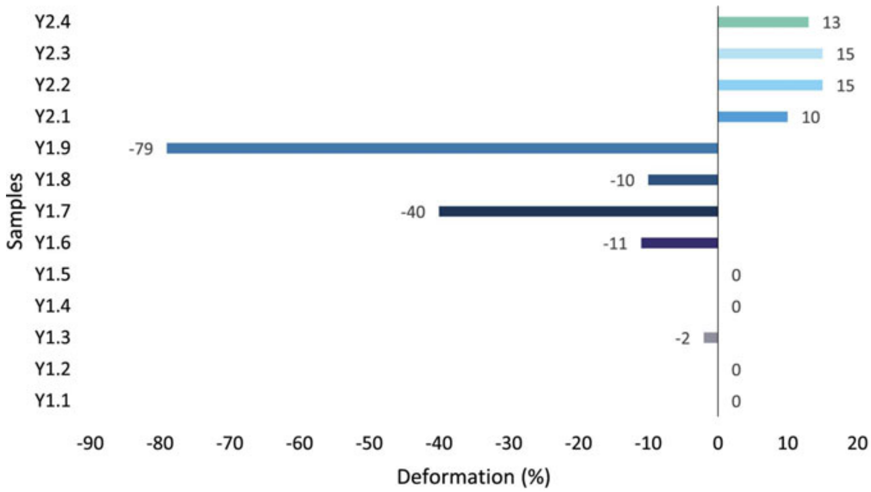

Figure 10. Deformation (%, negative values indicate shrinkage, positive ones indicate expansion) across G1 (manually extruded; Y1.1–Y1.9) and G2 samples (robotically 3D-printed; Y2.1–Y2.4) following environmental exposure. Note that because the deformation measurement methods differ across the groups, they are presented together for conceptual comparison only.

Wang *et al.* 2019). Regarding initial mass recovery after seven days of subsequent drying indoors, the G2 specimens' mass values were very close to the initial mass. The continued mass increase despite non-monotonic humidity variation suggests that while moisture availability is likely an influencing factor, it does not fully account for the observed trends, and additional factors such as material structure, layering, and fabrication-induced porosity may contribute.

Samples submerged in water (Y1.7, Y1.8, and Y1.9) exhibited a trend of rapid and high (up to 110%) mass accumulation within the first 10 minutes of immersion (Figure 8d, Table S5 in the Supplementary file). The mass gain was in this case significantly more pronounced than for the samples exposed outdoors. Sample Y1.7, after being submerged and subjected to stirring, became damaged and lost some of its surface area. After 10 minutes of stirring, the mass of that sample increased by 61%. After two days of drying indoors, the mass of the sample decreased below the initial value, and showed stable values on the seventh day. Sample Y1.8, exposed to passive water immersion with no stirring, increased its initial mass by 104% within the first 10 minutes. After seven days, its mass decreased below the initial value. To investigate this behavior further, a third sample (Y1.9) was submerged in the same amount of water and left in the medium for 24 hours. An increase in mass of 184% was observed. The sample was then allowed to dry, and the mass was measured after 2 days. The resulting mass decrease was −67%, in contrast with lower values (−21% and −45%) for samples exposed to shorter, 10-minute-long, submersion

Notably, these measurements should be interpreted with caution. The immersion experiments combined environmental and mechanical factors of exposure to liquid water and mechanical agitation through stirring, which cannot be fully isolated in the present setup. For sample Y1.7, the mass gain and mass loss values cannot be accurately estimated and compared due to partial sample disintegration during stirring. Although in the sample subjected to stirring the mass gain and loss effects might have been exacerbated by stirring-induced surface damage and partial material loss, the exposure to water and associated hydrostatic pressure might also have contributed, also for the other samples. Overall, the observed mass change behaviors likely result from a combination of physicochemical effects (e.g., plastic deformation of the hydrogel network during prolonged water exposure) and mechanical effects (e.g., structural disruption or material loss during stirring). This further highlights that, across the experimental scenarios, multiple interacting environmental and mechanical variables contribute to the observed mass changes, and their individual effects cannot be isolated within the current setup. Extended immersion may further amplify these changes through leaching of soluble components such as yeast, glycerol, and sodium alginate (Kamemaru *et al.* 2018), leading to partially irreversible mass changes. Consequently, the recorded weight variations should be considered approximate and not strictly comparable to the initial dry sample state. Despite these limitations, a consistent qualitative trend across all immersion conditions was the strong affinity of the material for water uptake.

Geometric deformation

2D deformation

For Group G1, deformation measurements for samples Y1.1 and Y1.2 maintained indoors showed shape stability over the seven-day observation period with no geometric deformation (Figure 10, Table S6 in the Supplementary file). The only outlier in this group was sample Y1.3 placed indoors on wet soil, which exhibited slight shrinkage (−2%). Deformation was localized primarily at the lower region of this sample, in the contact area with the substrate. Samples Y1.4 and Y1.5 exposed to outdoor conditions exhibited no deformation over time. The greatest shrinkage (−11%) in this exposure setting occurred in sample Y1.6 placed outdoors on wet soil.

The highest deformation values were registered in the water-submerged samples (Figure 11). Within this group, sample Y1.8 exhibited the lowest shrinkage (−10%), with deformation predominantly occurring along the perimeter. The greatest shrinkage (−79%) observed in sample Y1.9 can be potentially correlated with material fragmentation arising from structural fragilization due to prolonged immersion time. The second most deformed sample, Y1.7 (−40%), was subjected to continuous mechanical agitation during immersion. This suggests that the observed fragmentation reflects a combined effect of water saturation and external mechanical stress, rather than moisture exposure alone. Because water as a medium as well as stirring introduce mechanical forces absent in other exposure scenarios, the results from Y1.7 should be interpreted as illustrative of extreme combined hydraulic and mechanical conditions and are not directly comparable to passive immersion or atmospheric exposure.

3D deformation

For Group 2 (Y2.1–Y2.4), the digital calculations of distance deviations between the sample scans before and after environmental

https://doi.org/10.1017/S2977905726100262 Published online by Cambridge University Press

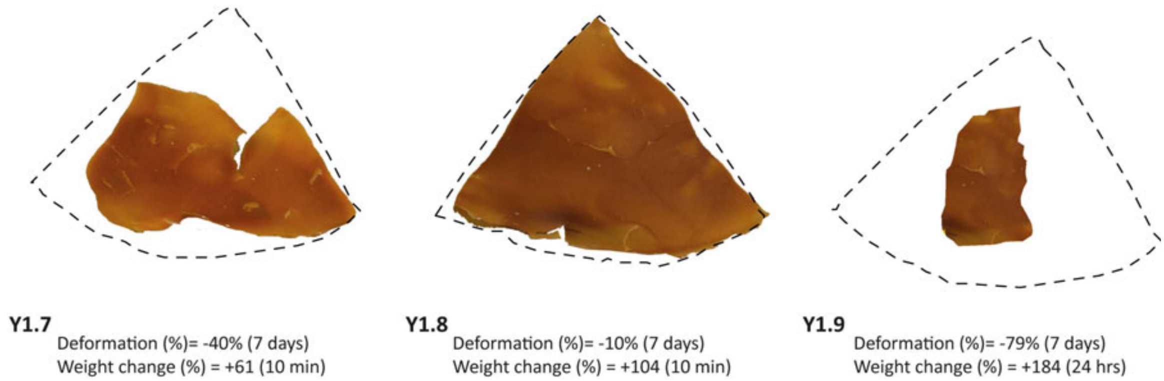

Figure 11. YCBH sample damage after immersion in water.

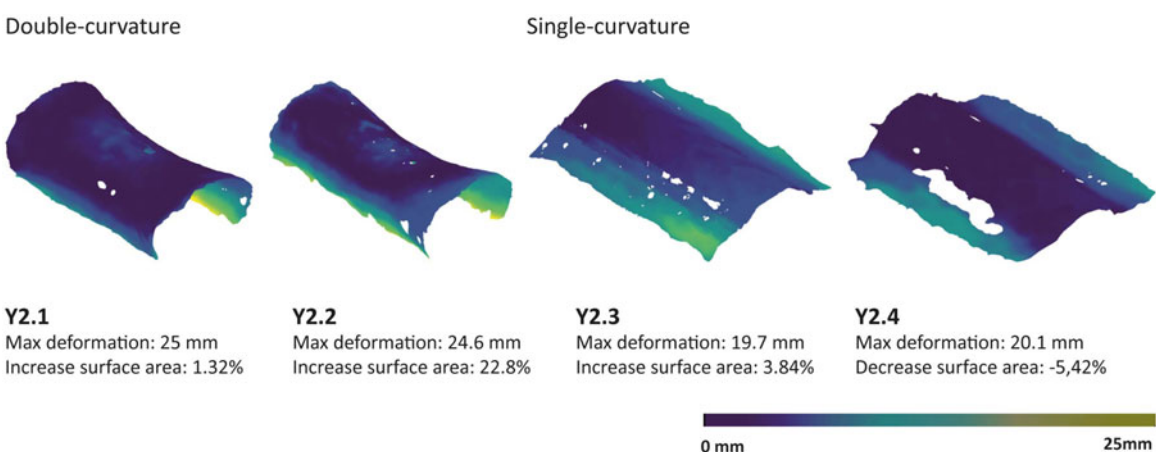

Figure 12. Digital analysis of shape deviations in single- and double-curved YCBH sample geometries.

exposure indicate greater resistance to deformation in samples with double curvature (Y2.1 and Y2.2), which exhibited an average geometric deformation of 12% (Figure 10, Table S7 in the Supplementary file). In contrast, simple-curvature samples (Y2.3 and Y2.4) showed higher average deformation of 14%.

Although both geometries maintained their overall structural configuration, the single-curved samples tended to flatten, whereas double-curved ones kept their global curved shapes and only exhibited reduced shape fidelity along longitudinal edges (Figure 12). The increased deformation in double-curvature samples (Y2.1, Y2.2) can be interpreted through their Gaussian curvature, which acts as a critical determinant of morphological stability during hydrogel dehydration. In these non-developable surfaces, the accumulation of anisotropic internal stresses was unable to find a linear path for stress relief. Consequently, while the central zones of the samples maintained stability due to geometric constraints, in the longitudinal edges the energy was dissipated, yielding significant distortion and loss of fidelity (Mitropoulou *et al.* 2025).

Thickness variation

Thickness measurements showed substantial increases in material thickness in the outdoor and submerged samples, ranging from 33% to 173%, depending on geometry, layering, and exposure condition (Figure 13, Table S8 in the Supplementary file). This trend aligns with mass change behaviors described in the earlier subsection, potentially explaining the concurrent increase in mass. Within Group 1, sample Y1.6, which was in direct contact with humid soil, exhibited the most significant thickness increase (70%) among the outdoor samples. In contrast, for samples Y2.1–Y2.4, the thickness substantially increased relative to the initial state, with a peak increase of 173% for sample Y2.2. This group is the only one featuring multiple printed layers, a characteristic that likely increased the water retention and mass accumulation capacity. Notably, while the submerged samples (Y1.7, Y1.8 and Y1.9) appeared to undergo more drastic overall changes of mass, their thickness variations remained more conservative on average compared to the multi-layered 3D printed samples.

Embrittlement assessment

While YCBH samples exposed outdoors (Y1.4–Y1.6, Y2.1–Y2.4) tolerated the imposed curvature without visible damage, samples submerged in water (Y1.7–Y1.9) exhibited visible cracking or fracture under the same deformation (Table 1). The imposed surface strain values during bending ranged between 0.30 and 1.50. No direct correlation was observed between sample thickness and embrittlement. Rather, immersion in water appeared to be the determining factor most likely causing damage in all submerged samples. This was seen as a reduction in flexural ductility for samples subjected to prolonged water exposure, suggesting a potential additional influence of moisture on structural fragilization.

https://doi.org/10.1017/S2977905726100262 Published online by Cambridge University Press

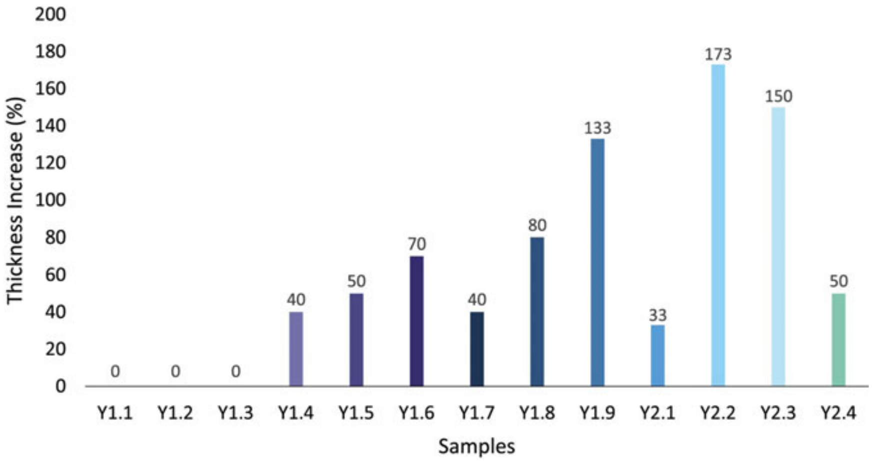

Figure 13. Thickness increase (%) across all samples from G1 and G2 measured in wet state following environmental exposure, relative to initial dry thickness.

Table 1. Embrittlement assessment of YCBH samples in Group 1

	Y1.1	Y1.2	Y1.3	Y1.4	Y1.5	Y1.6	Y1.7	Y1.8	Y1.9
0 = No visible cracking 1= Visible cracking 2 = Fracture	0	0	0	0	0	1	2	1	2
ε	0.45	0.60	0.45	0.75	0.30	1.50	0.75	0.75	0.45

Colorimetric analysis

Comparative analysis between the dry state recorded after seven days of indoor sample curing and the wet state observed on the seventh day of outdoor exposure revealed chromatic shifts in the material (Figure 14, Table S9 in the Supplementary file). These shifts are represented by the ΔE values, which for all analyzed samples were above the threshold of $\Delta E = 5$ which indicates that the observer perceives two distinct colors.

The two natural-colored samples without added pigments exhibited similar color difference values ΔE (22.6 for Y2.2 and 21.7 for Y2.4). In comparison, the two samples with added pigments showed lower ΔE values (6.5–18.7), which suggests that the presence of pigments could have reduced the chromatic shifts in these samples. Additionally, the large differences between the individual ΔE values registered in these samples for differently colored (white, red, black) sampling points further suggest that color stability could be additionally influenced by pigment concentration. When comparing samples Y2.2 and Y2.3, the results indicated that larger black pigment quantities used in the material formulation of sample Y2.3 (Table S1 in the Supplementary file) correlated with a significant decrease in its ΔE. Besides this, all samples presented a yellow base color due to the natural chromatic properties of yeast, reflected in consistently high positive b values in the LAB color space.

Discussion

From material transformation tendencies to architectural design applications

The experimentally observed time-dependent environmental responses of the yeast-cellulose biohydrogel samples, i.e., mass increase, moisture-driven swelling, edge-specific deformation, fragilization under prolonged wetting, and chromatic variation, demonstrate that the material does not behave as a typical stable construction material but as a temporally active material system. Rather than qualifying these transformations as limitations, this study positions them as design-relevant behaviors that can be deliberately modulated through strategic design choices for construct geometry, layering, environmental exposure, and substrate interaction.

In this sense, the material aligns with a paradigm of temporal, environmentally responsive and circular architecture, in which building elements are conceived as transient, adaptive, and biodegradable, to function within a cradle-to-cradle biomass circulation context. Architectural elements designed according to this circularity logic are not optimized for permanence, but for programmed transformation, maintenance, and eventual ecological return to the natural environment. The discussion below consolidates these implications based on the experimental material study results and translates them into explicit architectural design-relevant parameters, using the pavilion concept as a mediating and illustrative artifact.

The speculative pavilion

The pavilion is proposed as a translational artifact between research findings and design application. Thus, it is not a finalized, technically resolved and ready to be built architectural project. Its purpose is to explicitly connect the observed material behaviors to spatial, structural, and temporal design decisions at an architectural scale. The pavilion is assumed to operate within defined environmental thresholds and short lifecycles and is therefore suited to non-load-bearing installations, exhibition structures, or ecological interfaces.

The design is articulated as a system of pillars, each conceived as a bioresponsive architectural element (Figure 15). The pillars are designed to illustrate different life cycle scenarios and performative functions. Some are programmed for accelerated decay, and others for controlled maintenance or partial persistence. This differentiation mirrors metabolic processes found in biological systems, where growth, repair, and decomposition coexist within a single

https://doi.org/10.1017/S2977905726100262 Published online by Cambridge University Press

Figure 14. Chromatic shifts in robotically 3D printed YCBH samples after outdoor exposure.

organism or ecosystem. Crucially, each design parameter, i.e., geometry, layering, substrate contact, attachment detailing, pigmentation, is directly derived from material transformation tendencies observed in the physical experiments with the YCBA material.

Geometry as regulator of deformation and stability

Experimental results of the 2D and 3D deformation analyses of the material samples suggested that geometric deformation is most pronounced at exposed perimeters of the samples, while interior regions remain stable. Translating this insight into architectural design entails treatment of architectural component edges as active material transformation zones, either protected when dimensional stability is required, or intentionally exposed when spatial transition or degradation is desired.

The 3D deformation experiments further suggested that double-curved geometries appear more form-stable under wetting and drying cycles than single-curved shapes. This finding is reflected in

https://doi.org/10.1017/S2977905726100262 Published online by Cambridge University Press

Figure 15. Speculative architectural pavilion concept featuring (a) and (c) pillars programmed for bioresponsiveness, (b) tactile properties, (d) ecosystemic interaction with vegetation, insects, animals and microbes.

the pavilion design, with each pillar having a doubly curved, hyperbolic paraboloid geometry (Figure 16). This form is intended to function as a shell-like structure, creating an opportunity to distribute stresses, mitigate buckling, and potentially reduce collapse under material mass increase due to moisture uptake. Rather than heavily relying on traditional structural support frames, the pillar design speculates that geometric form enables extra stiffness and can thus partially compensate for the material's hygroscopic behavior. In this configuration, moisture-induced swelling and shrinkage are framed as a self-tensioning mechanism, stabilizing the form.

Programmable mass change, moisture regulation, and capillary action

For mass and thickness change aspects, the observations in the material experiments suggested correlations with layer number and configuration. Multilayered samples exhibited reduced mass increase under outdoor exposure, indicating that layering could function as a design parameter for moisture regulation. Framed in this way, layering could be used as a strategy to create a dedicated, separate material layer that serves as a scaffold for plants to climb and grow on, turning the pillar into an object that could supports colonization by specific plant species that would benefit from the YCBH material's moisture buffering properties (Figure 17, component 1). In the pavilion concept, this idea is further enabled through localized material reinforcement achieved via dedicated 3D printing strategies. Structural attachment zones and high-stress areas (Figure 17, components 1–3) are designed to be 3D printed as multiple superimposed layers, while other regions are intentionally kept thinner to make them more responsive. This differentiation would allow selected areas to maintain integrity while adjacent zones undergo controlled deformation or decay.

Regarding moisture regulation aspects, the material experiments have shown that exposure to humid and aquatic environmental conditions causes the material to increase its mass and soften, which might lead to physical and biochemical disintegration under prolonged exposure. In the pavilion design scenario of decay, this property is accommodated by allowing intentional material contact with moisture and rainwater, to allow its gradual breakdown. First, to act as a substrate for microbial metabolic activity, leading to partial decomposition into biomass, and then to transition fully into compost, providing a nutrient-rich substrate promoting plant growth (Figure 17, components 1 and 6).

Furthermore, the experiments for moist soil contact suggested that it is not a neutral exposure condition but an active interface that can potentially drive capillary moisture uptake, structural softening, and biodegradation. Accordingly, the pavilion design differentiates pillar bases based on intended lifecycle outcomes. Pillars designed for full degradation are placed directly in organic soil, whereas pillars intended for prolonged operation are separated through elevation above ground and inclusion of drainage around the structures (Figure 17, component 5). This explicit substrate differentiation clarifies how decay is not incidental but can be carefully programmed through ground contact. Soil interaction thus can become a design tool for staging disassembly, nutrient release, and ecological integration.

Moisture uptake and decay behaviors are traditionally treated as failure modes in construction materials. In this study, they are reframed as environmental actuators capable of shaping temporal architectural functionalities. Within the pavilion concept, mass change is intended to inform spatial and functional differentiation, and elements exposed to rainfall or embedded in soil are expected to swell, distort, or lose rigidity over time. Such behaviors could be harnessed architecturally to modulate porosity, daylight access, or enclosure (Figure 17, component 8). For instance, swelling elements may partially occlude openings during wet conditions, while drying cycles could restore permeability. In this sense, the presence of moisture and water becomes an active driver of spatial transformation rather than a destructive force.

https://doi.org/10.1017/S2977905726100262 Published online by Cambridge University Press

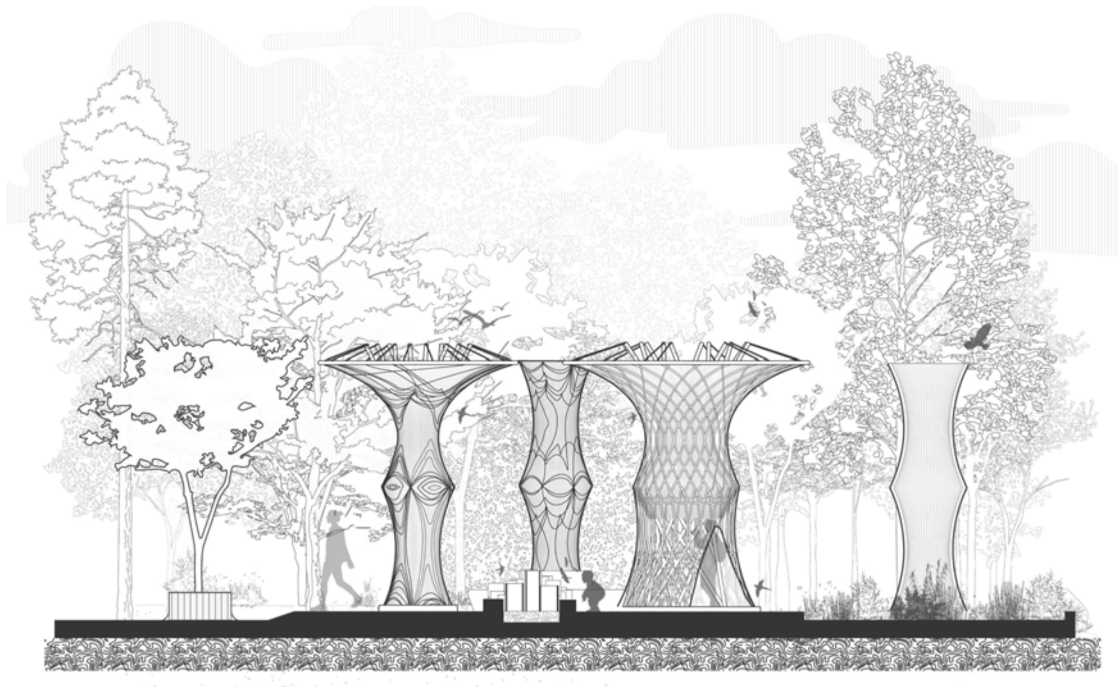

Figure 16. Pavillion pillar designs featuring doubly curved hyperbolic paraboloid geometry for enhanced structural stability.

Embrittlement and controlled disassembly

Experimental observations of flexural properties of the samples after exposure to different environmental conditions have suggested that prolonged water exposure may lead to embrittlement and loss of flexural strength in the YCBH material. Rather than resisting this behavior, the pavilion concept assumes that such fragilization could be engaged as a mechanism for controlled disassembly. Thin sections, targeted wetting zones, or moisture-retentive geometries could be designed to initiate cracking, delamination, or collapse at predefined moments. In architectural terms, such behavior could support designs where elements are meant to soften, open, or fail gradually, triggering transitions such as seasonal openness, scheduled replacement, or ecological transfer to the surrounding environment. Fragilization therefore contributes to a designed end-of-life scenario, shifting beyond uncontrolled and undesired material failure.

Chromatic transformation as environmental indicator

Chromatic changes between wet and dry states observed in the experiments provide a further incentive for implementing the agency of an architectural biomaterial in an ecological context. In the pavilion design, chromatic variation is employed not as decoration but as embedded environmental feedback. Unpigmented areas lighten upon moisture exposure, showing temporal changes in water flow paths, saturation zones, or soil-contact areas, allowing the material to act as a chromatic moisture sensor (Figure 18a). Beyond human perception, such chromatic change may also influence biotic interactions. In the context of evolutionary biology and sensory ecology, color can function as both attractor and deterrent. For example, high-saturation color or dark hues can signal toxicity, nutritional value, ripeness, or decay. Thus, strategic use of added pigments, as well as intentionally designed transition of natural color could mediate aposematic and honest signaling between species and their environment (Figure 18b).

Reversible transformations as precursors to designing with decay

The material transformations observed in the experiments suggest design relevance of both reversible and irreversible material transition scenarios. In the experiments, the partially reversible transformations of samples over time may be indicative of the capability of the material to accommodate more than one cycle of transitions, beyond a binary, unidirectional change of state from one to another. Sample behaviors suggest that swelling-shrinkage cycles, mass increase under intermittent moisture, and chromatic variation in the unpigmented constructs due to moisture uptake and release constitute at least partially reversible responses that could allow the material to adapt to environmental change without immediate loss of integrity. These behaviors could be harnessed as early-stage indicators and actuators, making environmental exposure legible and temporally regulated. Under sustained or intensified exposure, such as prolonged saturation or continuous soil contact, these reversible responses can transition into irreversible disintegration and decay processes discussed in the previous subsections, including embrittlement, structural weakening, and biodegradation. Designing with decay therefore does not oppose reversible transformation but builds upon it by permitting the reversible behaviors to condition, signal, and spatially localize the irreversible decay pathways activated through cumulative environmental interaction.

End-of-life, circularity, and regenerative potential

The pavilion proposal frames end-of-life as gradual transformation and reintegration within the concept of regenerative ecologies which foster conditions for different forms of life to thrive, evolve and restore in cycles (Figure 19). This concept replaces the conventional approach of contemporary construction practice, which is heavily reliant on a linear process of material extraction, use, demolition and landfill disposal, with carefully staged scenarios of

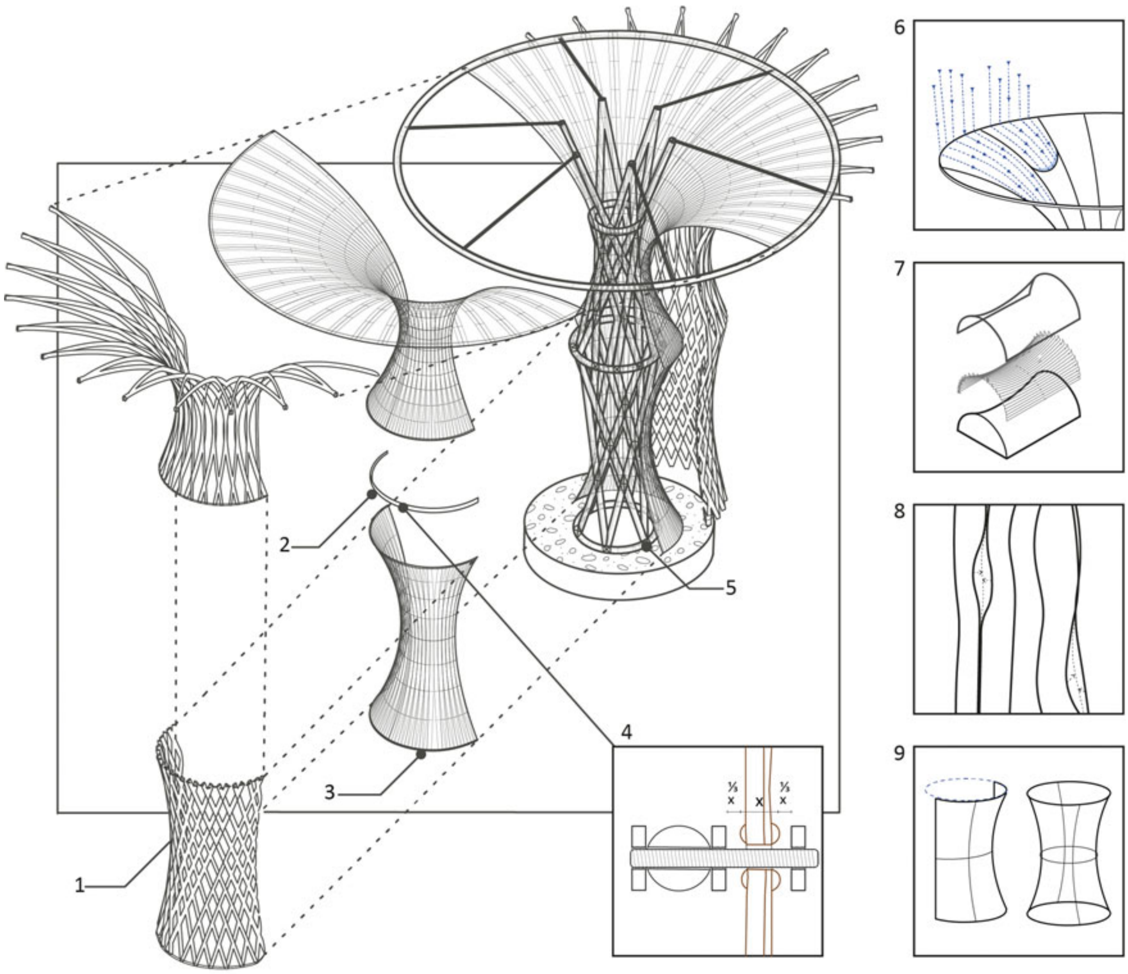

1. Layered paneling to regulate differential degradation over time.
2. Double toolpath reinforcement at joints to resist swelling stresses.
3. Base reinforcement to control excessive capillary uptake.
4. Attachment detail allowing expansion material thickness.
5. Drained foundation system to prevent water accumulation and prolong durability.
6. Toolpath design allowing/preventing water stagnation, supporting degradation or color change.
7. Layered 3D printing to control mass change and reinforcement.
8. Material expansion and shrinkage to allow aperture opening and closing.
9. Controlled borders in double curvature to enhance stability.

Figure 17. Pavillion pillar designed for temporal transformations and material decay.

biomass harvesting from industrial residues, short-term built structure use, maintenance, decay, and return to the environment through biodegradation. The pavilion pillars represent two speculative end-of-life scenarios. The first scenario is programmed for decay, with pillars meant to gradually soften, fragment, and ultimately merge with the soil, enriching the substrate by returning nutrients or serving as temporary scaffolds for vegetal growth. The second scenario is programmed for temporal, cyclic maintenance, with pillars meant to undergo cycles of repair, replacement or reinforcement, keeping the system operational while other elements decompose. In this second scenario, decay plays an enabling role rather than a terminal one, facilitating ecological succession and biomass circulation. Nevertheless, both scenarios remain conceptual and must be validated through further studies encompassing ecological assessment of aspects such as soil impact, species colonization, and nutrient release profiling.

Limitations and future research directions

While this study provides initial insights about environmental transformation behaviors of a yeast-cellulose biohydrogel, several constraints remain that limit generalization of the findings and require further extensive research. Firstly, the environmental exposure times in the experiments were short and therefore do not characterize the material's long-term behavior, including seasonal cycling, microbial colonization, UV exposure, and freeze-thaw effects. The sample size was also insufficient to achieve statistical reliability of the findings. Consequently, the numerical findings registered for mass change, deformation, embrittlement and color change should be treated as early-stage indicators of material tendencies rather than exhaustive and final material characterizations.

Further, the environmental conditions (humidity, soil contact, water immersion) in the experiments were intentionally simplified,

https://doi.org/10.1017/S2977905726100262 Published online by Cambridge University Press

Figure 18. Examples of pillar designs programmed for (a) color and form decay, and (b) continuous maintenance, plant symbiosis and ecosystemic signaling through deliberately designed color selection.

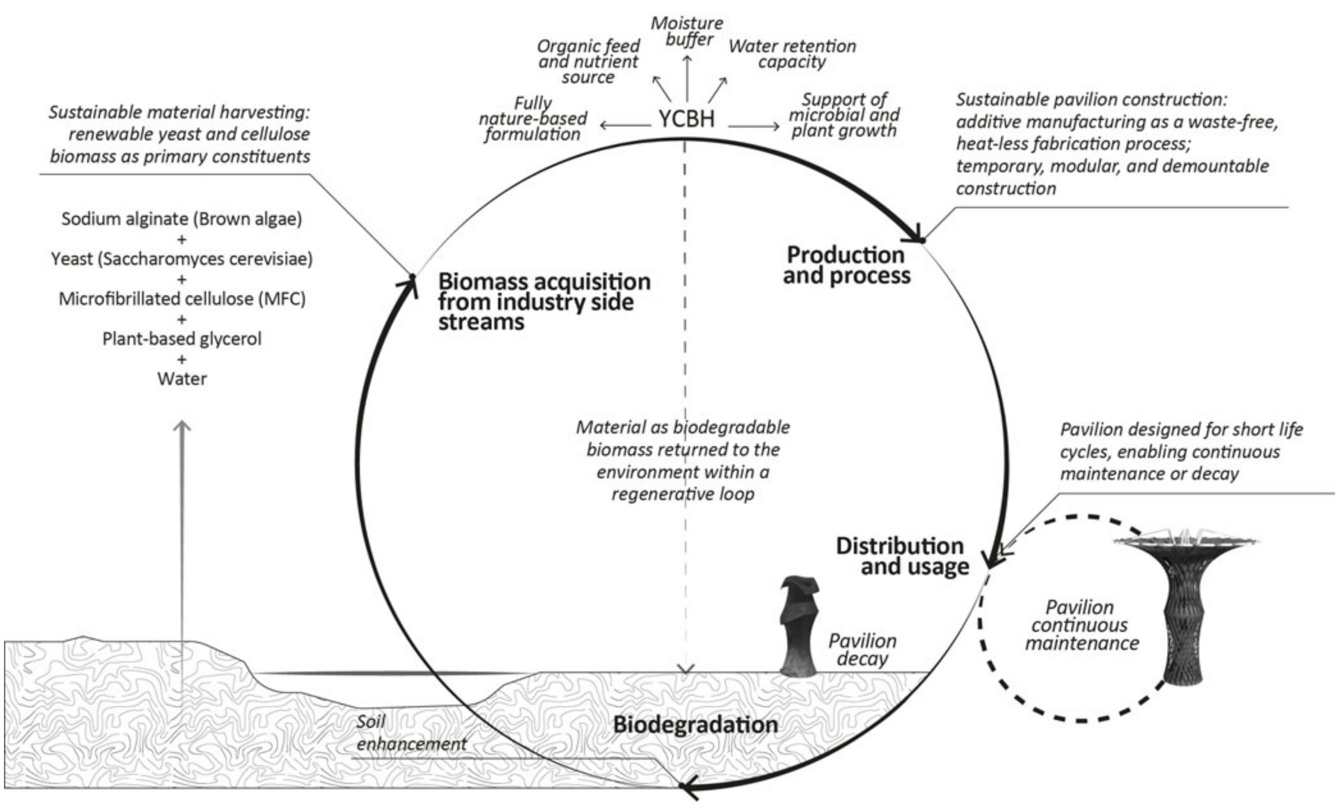

Figure 19. End-of-life, circularity, and regenerative potential aspects of design for decay implemented in the speculative pavilion made from the YCBH material.

and due to the intent of representing real-world conditions, not fully controlled and constant. These settings still do not fully represent the breadth and heterogeneity of real-world architectural environments, in which temperature and humidity fluctuations, soil chemistry, microbial diversity, rainfall frequency, or airborne particulate loads may significantly alter material responses.

https://doi.org/10.1017/S2977905726100262 Published online by Cambridge University Press

Table 2. Material experimentation results mapped to architectural design parameters and applications

Experimental result (observed behavior)	Underlying material mechanism	Design parameter(s)	Architectural implication	Implementation in pavilion concept
Moisture-induced mass increase	Moisture absorption	Degree of exposure to rain/humidity; material mass	Anticipated dimensional change; mass change as actuator	Pillars operate within defined environmental thresholds; mass increase allowed in non-critical zones, restrained at connections (Figure 17, component 7)
Accelerated mass increase in multilayer constructs	Material density; moisture absorption capacities; local material accumulation	Number of printed layers; layering density; local reinforcement	Layering as regulator of moisture uptake and deformation	Attachment zones reinforced with ≥2 layers, while other regions remain single-layered to enable transformation (Figure 17, components 1–3)
Localized decay at soil interface	Combined chemical, biological, and mechanical breakdown	Intentional weakness zones; substrate coupling	Decay as enabler of spatial opening, disassembly, and ecological transfer of biomass/nutrients	Base zones soften and fragment, enabling plant growth, microbial colonization, or material return to soil (Figure 15d)
Wet soil-induced capillary action	Upward moisture transport; continuous saturation	Substrate contact; soil composition; drainage layers	Ground contact as designed interface for persistence and/ or decay	Pillar bases alternately embedded in organic soil (decay) or isolated with drainage layers (persistence) (Figure 17, component 5)
Disintegration under prolonged water immersion	Loss of structural integrity due to sustained saturation and agitation	Exposure duration; immersion vs. intermittent wetting	Full immersion as end-of-life threshold	Pavilion designed for short-term, non-load-bearing use; collapse accepted as terminal state for specific elements (Figure 18a)
Thickness increase/swelling	Volume expansion of hydrated hydrogel	Accommodation in joints; swell-compliant mounting systems	Rigid fixings avoidance; inclusion of tolerances for material expansion	Enlarged head detail in wooden substructure designed to allow thickness expansion (Figure 17, comps. 2 and 4)
Moisture-induced embrittlement	Material weakening under prolonged saturation	Section thickness; wetting duration; water retention zones	Material weakening as mechanism for timed disassembly	Thin zones positioned in runoff or soil-contact areas to initiate cracking, softening, or collapse over time (Figure 17, component 6)
Swelling-shrinkage cycles	Cyclic hydration and drying	Environmental cycling tolerance	Swell and shrinkage as designed temporal behaviors	Pavilion as a system requiring monitoring, maintenance, and replacement, mimicking biological metabolism (Figure 18b)
Enhanced shape retention in double-curved 3D geometries	Shell-like stress distribution; curvature-based stiffness	Degree of curvature (single vs. double)	Geometric design (double curvature) as structural reinforcement	Hyperbolic paraboloid pillar geometry used to create self-supporting, frame-independent elements (Figure 17, component 9)
Edge-specific deformation	Differential drying; higher exposure at perimeter	Edge exposure; boundary geometry; local thickness	Perimeters as active transformation zones; edges designed for protection or controlled exposure	Pillar edges either shielded via strategic geometric design or intentionally exposed to promote decay and opening over time (Figure 17, components 9 and 8)
Chromatic shift between wet and dry states	Optical change due to water presence; biocomponent leaching	Natural color; surface exposure; moisture gradients	Color as environmental sensor	Pillars show moisture patterns and transformation stages via visible color change (Figure 18a)
Distinct chromatic behavior with added pigments	Differential pigment retention and color shift	Pigment quantity, type, distribution	Color as ecological signal	Pigmented pillars marked for decay vs. maintenance; color communication over time (Figure 18)

Similarly, the initial substrate interactions observed, such as capillary moisture uptake, cannot yet be extrapolated to all ground conditions or architectural interfaces.

Scaleup limitations also apply. The small sample geometries allow measurement of mass change, deformation, and chromatic transitions, but they cannot reproduce the structural complexity or load distribution of large architectural components. Material behavior under bending, self-weight, attachment detailing, or cumulative hydration gradients is likely to differ at 1:1 scale. Thus, while the design interpretations seek to accommodate the experimentally observed behaviors, they will remain speculative until validated through extensive prototyping, replication and multi-week/month outdoor deployment.

Methodologically, the reliance on simplified analytical approaches limits result accuracy. For instance, the digital image-based colorimetry introduces perceptual variability, and while sufficient for documenting large chromatic shifts, it does not match the precision of spectrophotometric methods. Likewise, the mass change and deformation measurements quantify bulk tendencies but do not provide deeper insight into microstructural changes, leaching kinetics, or biochemical breakdown of the material that would be required for a full biodegradation assessment. Future work should integrate spectrophotometry, microscopy, and biochemical assays to better characterize material breakdown.

Finally, while the material is framed as circular and regenerative, ecological costs of fabrication, of both the material and

https://doi.org/10.1017/S2977905726100262 Published online by Cambridge University Press

architectural components, including upstream resource flows, biomass processing, and energy use, were not quantified. Claims of sustainability and regeneration therefore require comprehensive life cycle assessment and ecological validation.

Synthesis

Despite its limitations, the experimental findings suggest that the yeast-cellulose biohydrogel exhibits transformation behaviors that could be relevant for future temporary and circular architectural applications. When linked to architectural parameters, i.e., geometry, layering, substrate contact, pigmentation, and attachment detailing, the observed behaviors can be translated into architectural designs that follow circular design thinking by featuring structures which are temporal, responsive, and biodegradable by design. To make the translation from experimental findings to architectural design parameters explicit, Table 2 synthesizes the observed material transformations and maps them to design variables, architectural implications and specific design strategies implemented in the pavilion concept. This mapping aims to synthesize the translational approach of this study, which could serve as a baseline example for further research cases and future applications of biomaterials in architecture and related biodesign fields.

Conclusion

This work contributes to biodesign research by demonstrating how systematic, design-situated material characterization can generate actionable material knowledge before full technological material optimization. In addition, by empirically documenting temporal material behaviors under semi-controlled but ecologically relevant conditions, the study exemplifies a biodesign approach in which material transformation, decay, environmental coupling, and limited predictability are legitimate objects of research inquiry. A yeast-cellulose biohydrogel served as a model material through which temporal processes were made observable, comparable, and translatable into design parameters.

The experimental findings did not only help understand the behaviors and tendencies of the studied biogenic material under environmental exposure but also allowed to show that the yeast-cellulose biohydrogel can as a temporally active material system, relevant for circular architectural design applications. Observed behaviors, including partially reversible mass fluctuation, swelling and shrinkage cycles, edge-specific deformation, capillary moisture transfer, moisture-induced fragilization, and visually perceptible color change, indicate that environmental responsiveness is intrinsic to the material. Rather than treating these behaviors as performance deficits, the study positioned them as material capabilities that can be selectively engaged. The experimental results suggested that design parameters including geometry, material deposition and layering, substrate contact, and pigmentation can be correlated with the observed material responses and purposefully engaged to steer the material toward stability or toward accelerated transformation and decay. Importantly, however, due to the lack of statistical replication and the foundational nature of the investigation, all findings should be regarded as preliminary, exploratory and indicative of material tendencies rather than final material characteristics.

By translating the empirically characterized transformation patterns into a speculative architectural pavilion scenario, the study illustrates how time-dependent material behavior can inform circular design strategies that operate within defined environmental thresholds and short life cycles. The pavilion is proposed as a translational artifact that links measured and observed material behaviors to spatial, geometric, and lifecycle design decisions. In this way, material transitions occurring due to environmental exposure over time are demonstrated as generative parameters for material-led design, rather than as failures to be eliminated.

In summary, the study demonstrates how material transformation and decay behaviors can be rendered legible and actionable through design-situated material characterization, highlighting the paramount role of biodesign research as a critical bridge between emerging biomaterials and regenerative design applications.

Supplementary material. The supplementary material for this article can be found at https://doi.org/10.1017/S2977905726100262

Data availability statement. The authors confirm that the data supporting the findings of this study are available within the article and its supplementary file.

Acknowledgements. The authors would like to acknowledge the technical assistance of Yagmur Bektas in biomaterial preparation and robotic 3D printing. The authors would also like to thank the sustainable biorefinery Borregaard for the microfibrillated cellulose sample provision for the prototyping experiments. During the preparation of this work the authors used Microsoft Copilot to improve grammar and text coherence. After using this tool, the authors reviewed and edited the content as needed and take full responsibility for the content of the publication.

Author contributions. Conceptualization: C.Q.; M.A.Z. Data curation: C.Q.; M.A.Z. Formal analysis: C.Q.; M.A.Z. Funding acquisition: M.A.Z. Investigation: C.Q. Methodology: M.A.Z. Project administration: M.A.Z. Resources: M.A.Z. Supervision: M.A.Z. Validation: M.A.Z. Visualization: C.Q.; M.A.Z. Writing – original draft: C.Q; M.A.Z. Writing – review & editing: C.Q; M.A.Z. All authors approved the final submitted draft.

Financial support. This work was supported by the Swedish Energy Agency (grant numbers P2022-00865, P2024-02409).

Competing interests. None.

Ethics standards. Ethical approval and consent are not relevant to this article type.

References

Aeby X, Bourely J, Poulin A, Siqueira G, Nyström G and Briand D (2023). Printed humidity sensors from renewable and biodegradable materials. *Advanced Materials Technologies* **8**(5), 2201302. https://doi.org/10.1002/admt.202201302.

Alonso CP (2021) Deep-time architecture: Building as material-event. *Journal of Architectural Education* **75**(1), 142–144. https://doi.org/10.1080/10464883.2021.1859906.

Anggraini W (2025) Development of biodegradable materials for consumer product packaging: Environmental impact and consumer preferences. *Journal Pijar Mipa* **20**(2), 304–310. https://doi.org/10.29303/jpm.v20i2.8588.

Arnardottir TH, Wang C, Haystead J, Eiriksdottir SS, Zhang M and Dade-Robertson M (2026) Formation finding: Exploring soft cast MICP fabrication in a water kiln. *Biotechnology Design* **4**, e5. https://doi.org/10.1017/S297790572510005X.

Barati B and Karana E (2019) Affordances as materials potential: What design can do for materials development. *International Journal of Design* **13**(3), 105–123. https://www.ijdesign.org/index.php/IJDesign/article/view/3419/879.

Bektas Y, Zboinska MA, Geijer C, Nypelö T and Hefny Z (2026a) Novel 3D printable yeast-based materials for architectural applications. *Frontiers of Architectural Research*. https://doi.org/10.1016/j.foar.2026.01.003.

Bektas Y, Zboinska MA, Skånberg Dahlstedt T, Geijer C and Nypelö T (2026b) Digital crafting of architectural biomaterials: computational geometric design and robotic 3D printing of yeast-cellulose hydrogels. In Proceedings of the 31st International Conference of the Association for Computer-Aided Architectural Design Research in Asia (CAADRIA), Hsinchu, Taiwan, 29 April–1 May 2026, Volume 2, pp. 205–214. https://papers.cumincad.org/cgi-bin/works/Show?caadria2026_353.

Chayaamor-Heil N, Perricone V, Gruber P and Guéna F (2023) Bioinspired, biobased and living material designs: A review of recent research in architecture and construction. *Bioinspiration & Biomimetics* **18**(4), 041001. https://doi.org/10.1088/1748-3190/acd82e.

Chen Z, Aziz T, Sun H, Ullah A, Ali A, Cheng L, Ullah R and Khan FU (2023) Advances and applications of cellulose bio-composites in biodegradable materials. *Journal of Polymers and the Environment* **31**(6), 2273–2284. https://doi.org/10.1007/s10924-022-02561-8.

Choi H-I and Yi H (2024) Biofabrication in architecture: 3D bioprinting of nature-sourced multi-material powder hydrogels, material testing, and prototyping. *Journal of Building Engineering* **87**, 109122. https://doi.org/10.1016/j.jobe.2024.109122.

Crawford A (2023) *Designer's Guide to Lab Practice*. London: Routledge. https://doi.org/10.4324/9781003363774.

Dade-Robertson M (2020) *Living Construction*. London: Routledge. https://doi.org/10.4324/9780429431807.

Elsacker E, Vandelook S, Brancart J, Peeters E and Laet LD (2019) Mechanical, physical and chemical characterisation of mycelium-based composites with different types of lignocellulosic substrates. *PLoS One* **14**(7), e0213954. https://doi.org/10.1371/journal.pone.0213954.

Elsacker E, Zhang M and Dade-Robertson M (2023) Fungal engineered living materials: the viability of pure mycelium materials with self-healing functionalities. *Advanced Functional Materials* **2023**(33), 2301875. https://doi.org/10.1002/adfm.202301875.

Ercan Ý (2025) Biodegradation in design process: digital building catalog for bio-inspired design proposals. In Proceedings of the 43rd Conference on Education and Research in Computer Aided Architectural Design in Europe (eCAADe 2025), Ankara, 1–5 September 2025, Volume 2, pp. 295–304. https://papers.cumincad.org/cgi-bin/works/Show?ecaade2025_410.

Fouad D, and Farag M (2020) Design for sustainability with biodegradable composites. In Yasa E, Mhadhbi M, Santecchia E (eds), *Design and Manufacturing*. IntechOpen. https://doi.org/10.5772/intechopen.88425.

Han Y, Wang S, Cao Y, Singh GP, Loh SI, Cheerlavancha R, Ang MC-Y, Khong DT, Chua PWL, Ho P, Strano MS and Marelli B (2023) Design of biodegradable, climate-specific packaging materials that sense food spoilage and extend shelf life. *ACS Nano* **17**(9), 8333–8344. https://doi.org/10.1021/acsnano.2c12747.

Ilomuanya MO (2020) Hydrogels as biodegradable biopolymer formulations. In Pal K, Banerjee I, Sarkar P, Kim D, Deng W-P, Dubey NK, Majumder K (eds), *Biopolymer-Based Formulations*. Elsevier, pp. 561–585. https://doi.org/10.1016/B978-0-12-816897-4.00023-0.

Kamemaru K, Usui S, Hirashima Y and Suzuki A (2018) Irreversible swelling behavior and reversible hysteresis in chemically crosslinked poly (vinyl alcohol) Gels. *Gels* **4**(2), 45. https://doi.org/10.3390/gels4020045.

Karana E, Blauwhoff D, Hultink E-J and Camere S (2018) When the material grows: A case study on designing (with) mycelium-based materials. *International Journal of Design* **12**(2), 119–136. https://ijdesign.org/index.php/IJDesign/article/viewFile/2918/817.

Kim J, Kim R, Martins J and Karana E (2024) Becoming microbes: an approach to cultivating microbial sensibilities in biodesign. In DRS2024: Boston, 23–28 June, Boston, USA. https://doi.org/10.21606/drs.2024.950.

Lazaro Vasquez ES, Ofer N, Wu S, West ME, Alistar M and Devendorf L (2022) Exploring biofoam as a material for tangible interaction. InMueller FFGreuter S, Khot RA, Sweetser P, Obrist M (eds), *Proceedings of the 2022 ACM Designing Interactive Systems Conference*. New York, NY, USA: Association for Computing Machinery, pp. 1525–1539. https://doi.org/10.1145/3532106.3533494.

Ling AS (2018) Design by decay, decay by design (Thesis). Massachusetts Institute of Technology. 23 February 2026. Available at https://dspace.mit.edu/handle/1721.1/120696.

Malik S, Hagopian J, Mohite S, Lintong C, Stoffels L, Giannakopoulos S, Beckett R, Leung C, Ruiz J, Cruz M and Parker B (2020) Robotic extrusion of algae-laden hydrogels for large-scale applications. *Global Challenges* **4**(1), 1900064. https://doi.org/10.1002/gch2.201900064.

Mitropoulou I, Bernhard M and Dillenburger B (2025) Curvature-informed paths for shell 3D printing. [Application/pdf] 15 p. https://doi.org/10.3929/ETHZ-B-000720105.

Mokrzycki W and Tatol M (2011) Color difference Delta E – A survey. *Machine Graphics and Vision* **20**, 383–411.

Mostafavi M and Leatherbarrow D (1993) *On Weathering: The Life of Buildings in Time*. Cambridge, MA, USA: MIT Press.

Mukherjee C, Varghese D, Krishna JS, Boominathan T, Rakeshkumar R, Dineshkumar S, Brahmananda Rao CVS and Sivaramakrishna A (2023) Recent advances in biodegradable polymers – Properties, applications and future prospects. *European Polymer Journal* **192**, 112068. https://doi.org/10.1016/j.eurpolymj.2023.112068.

Napier IM (2022) Robotically printed seaweed as a biomaterial within architecture and design. In van Ameijde J, Gardner N, Hyun KH, Luo D, Sheth U (eds), *POST-CARBON - Proceedings of the 27th CAADRIA Conference*. Sydney, Australia: The Association for Computer-Aided Architectural Design Research in Asia (CAADRIA). 9–15 April 2022, pp. 303–312. https://doi.org/10.52842/conf.caadria.2022.2.303.

Nicolae M, Roussel V, Koelle M, Huron S, Steimle J and Teyssier M (2023) Biohybrid devices: Prototyping interactive devices with growable materials. In Follmer S, Han J, Steimle J, Riche NH (eds), *Proceedings of the 36th Annual ACM Symposium on User Interface Software and Technology*. New York, NY, USA: Association for Computing Machinery, pp. 1–15. https://doi.org/10.1145/3586183.3606774.

Panagiotidou V, Koerner A, Cruz M, Parker B, Beyer B and Giannakopoulos S (2022) 3D extrusion of multi-biomaterial lattices using an environmentally informed workflow. *Frontiers of Architectural Research* **11**(4), 691–708. https://doi.org/10.1016/j.foar.2022.06.010.

Pettinelli N, Sabando C, Rodríguez-Llamazares S, Bouza R, Castaño J, Valverde JC, Rubilar R, Frizzo M and Recio-Sánchez G (2024) Sodium alginate-g-polyacrylamide hydrogel for water retention and plant growth promotion in water-deficient soils. *Industrial Crops and Products* **222**, 119759. https://doi.org/10.1016/j.indcrop.2024.119759.

Risseeuw C, Mcquillan H, Martins J and Karana E (2024) (Re)activate, (re) direct, (re)arrange: exploring the design space of direct interactions with flavobacteria. In Mueller FF, Kyburz P, Williamson JR, Sas C, Wilson ML, Toups Duga P, Shklovski I (eds), *Proceedings of the 2024 CHI Conference on Human Factors in Computing Systems*. New York, NY, USA: Association for Computing Machinery, pp. 1–18. https://doi.org/10.1145/3613904.3642262.

Rudin R, Zboinska MA, Sämfors S and Gatenholm P (2022) Reprint: digital workflow for aesthetic retrofitting of deteriorated architectural elements with new biomaterial finishes. In Hybrids and Haecceities, Proceedings of the 42nd Annual Conference of the Association of Computer Aided Design in Architecture (ACADIA). University of Pennsylvania Stuart Weitzman School of Design, pp. 336–345. https://papers.cumincad.org/cgi-bin/works/paper/acadia22_336.

Sannino A, Demitri C and Madaghiele M (2009) Biodegradable cellulose-based hydrogels: Design and applications. *Materials* **2**(2), 353–373. https://doi.org/10.3390/ma2020353.

Skrzypczak D, Mikula K, Kossińska N, Widera B, Warchoł J, Moustakas K, Chojnacka K and Witek-Krowiak A (2020) Biodegradable hydrogel materials for water storage in agriculture - Review of recent research. *Desalination and Water Treatment* **194**, 324–332. https://doi.org/10.5004/dwt.2020.25436.

Song KW, Bell F, Deshpande H, Mandel I, Wun T, Alistar M, Buechley L, Ju W, Kim J, Paulos E, Sabie S and Wakkary R (2024) Sustainable unmaking: Designing for biodegradation, decay, and disassembly. In Yamashita N, Evers V, Yatani K, Ding XS (eds), *Extended Abstracts of the CHI Conference on Human Factors in Computing Systems*. New York, NY, USA: Association for Computing Machinery, pp. 1–7. https://doi.org/10.1145/3613905.3636300.

Stefanova A, Bridgens B, In-na P, Caldwell G and Armstrong R (2020) Architectural laboratory practice for the development of clay and ceramic-based photosynthetic biocomposites. *Technology|Architecture + Design* **4**(2), 200–210. https://doi.org/10.1080/24751448.2020.1804764.

Stickney C (2023) An architecture of decay: Addressing building waste through biologically integrated architecture (Thesis). Lawrence Technological University. 23 February 2026. Available at https://ltu.edu/wp-content/uploads/2026/02/Stickney_Report.pdf.

Tai Y-JT, Bader C, Ling AS, Disset J, Darweesh B, Duro-Royo J, Van Zak J, Hogan N and Oxman N (2018) Designing (for) decay: Parametric material distribution for hierarchical dissociation of water-based biopolymer composites. *Proceedings of IASS Annual Symposia* **2018**(9), 1–8.

Valverde Rojas MC, Österreicher D, Fischer LK and Knippers J (2026) Thermal regulation in urban surfaces: evaluating 3D-printed porous geometries for wild bee nesting aids. *Biotechnology Design* **4**, e7, 1–14. https://doi.org/10.1017/S2977905726100079.

Wang X, Zhao L, Fuh JYH and Lee HP (2019) Effect of porosity on mechanical properties of 3D printed polymers: Experiments and micromechanical modeling based on X-ray computed tomography analysis. *Polymers* **11**(7), 1154. https://doi.org/10.3390/polym11071154.

Zboinska MA, Sämfors S and Gatenholm P (2023) Robotically 3D printed architectural membranes from ambient dried cellulose nanofibril-alginate hydrogel. *Materials & Design* **236**, 112472. https://doi.org/10.1016/j.matdes.2023.112472.

Zboinska MA (2025) Biobased coatings for architectural timber applied using the robotic 3D printing technique. *Architectural Science Review* **68**(6), 449–466. https://doi.org/10.1080/00038628.2024.2427711.

Zhou J, Doubrovski Z, Giaccardi E and Karana E (2024) Living with cyanobacteria: Exploring materiality in caring for microbes in everyday life. In *Proceedings of the 2024 CHI Conference on Human Factors in Computing Systems*. New York, NY, USA: Association for Computing Machinery, pp. 1–20. 23 February 2026. https://doi.org/10.1145/3613904.3642039.

Zowada R and Foudazi R (2023) Macroporous hydrogels for soil water retention in arid and semi-arid regions. *RSC Applied Polymers* **1**(2), 243–253. https://doi.org/10.1039/D3LP00117B.